Hindawi
Shock and Vibration
Volume 2023, Article ID 6675678, 30 pages
https://doi.org/10.1155/2023/6675678

Research Article

Corotational Finite Element Dynamic Analysis of Space Frames with Geometrically Nonlinear Behavior Based on Tait–Bryan Angles

Ahmed A. H. Elerian, Saiid A. Shebl, and Hesham A. Elkaranshawy

Department of Engineering Mathematics and Physics, Faculty of Engineering, Alexandria University, Alexandria, Egypt

Correspondence should be addressed to Hesham A. Elkaranshawy; hesham_elk@alexu.edu.eg

Received 5 April 2023; Revised 20 July 2023; Accepted 2 August 2023; Published 2 September 2023

Academic Editor: Salvatore Caddemi

The aim of this study is to compose a corotational finite element formulation for space frames with geometrically nonlinear behavior under dynamic loads. Using a moving frame through three successive rotations similar to Euler angles is one of the oldest techniques; however, there are still some gaps that require attention, mainly due to singularity. Hence, alternative techniques had been developed, sometimes elusive and computationally expensive. In this paper, we went back to the old technique and filled the gaps. Three-coordinate systems are used, i.e., the fixed global coordinate system, the fixed local coordinate system that is attached individually to every element, and the corotational local frame for each element that moves and rotates with the element. The deformation is always small relative to the corotational frame. The successive rotations between different coordinate systems are expressed using Tait–Bryan angles. Lagrange's equation is used to derive the equation of motion, and the stiffness and mass matrices are obtained using the Euler–Bernoulli beam model. A MATLAB code is developed based on the Newton–Raphson method and the Newmark direct integration implicit method. In traditional techniques, singularity is attained when any rotation angle in the fixed local frame approaches $\pi/2$, and if any is greater than $\pi/2$, the techniques could fail to specify the location of the element. In this paper, each case is treated with a proper procedure, and special handling of trigonometric formulations prevents singularity and correctly specifies the location of elements in all situations. Different examples of beams and frames are analysed. While the method is not intricate, it is timesaving, is highly effective, provides more stable and robust analysis, and gives sufficiently accurate results. Compared to the parametrization of the finite rotations technique, the method has a significant reduction in the convergence rate because it avoids the storage of joint orientation matrices.

1. Introduction

In recent years, the development of lightweight high-strength materials has attracted many industries [1–3]. No wonder, industry always faces new challenges and needs to reduce the cost of designs. Such designs inevitably experience large displacements but with small strain. That is why geometrically nonlinear analysis plays a crucial role in such designs, which cannot be analysed using the traditional linear analysis. Remarkably, it remains a fertile ground for research due to the continuous demand for accurate, adaptable, and computationally inexpensive geometrically nonlinear formulations for treating innovative applications. To elucidate this point, Leng et al. [4] pointed to the significant effect of the geometric nonlinearity on the flexible offshore structures and devices that cannot be ignored. Trapper [5] studied a pipe lay on a seafloor that experienced large deformations. Accordingly, he used a geometrically nonlinear model to calculate the maximum internal forces locations. Liu [6] investigated a geometrically nonlinear finite element formulation to determine the dynamic response of a guyed transmission line system that contains large displacements from the vibration of cables. With the unprecedented growth in renewable energy, increasing the scale of renewable energy devices becomes an urgent need. As a result, Xiaohang et al. [7] analysed a 100-meter flexible

wind turbine blade. This investigation reveals that geometric nonlinearity plays an indispensable role in the computation of the dynamic response of such giant blades. Due to the increasing interest in deep space exploration, there is a continuous need for space applications and habitats. It is worthy to say that such applications of light-weight materials contain large displacements. Therefore, Liu and Bai [8] considered the geometric nonlinearity during their experimental and numerical investigation of a deployable composite cabin for space habitats. The important question that can be addressed here is why shall we develop geometrically nonlinear models in the existing of various finite element commercial softwares? The answer is not complicated; there is still a need to investigate more versatile, efficient, and time-saving models that can successfully handle different engineering problems which may be exclusive or intractable in some cases using these commercial programs.

According to Crisfield [9], Turner et al. [10] were the first to study geometrically nonlinear finite element analysis in the sixtieths of the last century. In fact, Argyris [11] made considerable premature contributions in genuine geometrically nonlinear analysis procedures. Essentially, the geometrically nonlinear finite element analysis of structures was covered in some notable books by Oden [12], Bathe [13], and Crisfield [9].

In general, there are two different forms, in continuum mechanics, to describe the motion of a body, namely, Eulerian and Lagrangian formulations. The Eulerian formulations are usually used in fluid mechanics, while Lagrangian formulations are used in most other engineering fields. With regard to geometrically nonlinear analysis, the Lagrangian formulations are commonly used in the form of total Lagrangian, updated Lagrangian, and corotational formulations. In total Lagrangian formulations [14–17], the system equation terms are defined in terms of the fixed global frame that does not change through the analysis. This generates relatively large strains, displacements, and rotations that need special procedures to handle.

While in updating Lagrangian formulations [18, 19], the terms of the equation are defined relative to a frame that is updated with the last accepted solution. This reference frame does not change during the solution cycles. As a result, the system equations are much simpler than the corresponding equations in total Lagrangian formulations. However, if the displacement from the current configuration to the last equilibrium configuration is large, a basic assumption is violated and accordingly these formulations experience also some complexities. To avoid such complexities, corotational formulations [20–31] provide a simple kinematics description method for large displacement analysis. These formulations are based on the theory of small strain. The corotational local frame translates and moves with each element but does not deform with it. Consequently, one obvious advantage of this formulation is that it can easily filter the rigid-body motion from the deformational motion, which is always small relative to the corotational local frame. This frame, which is continuously updated, can be defined by many different methods [23]. Remseth [17] used an approximate vectorial assumption to deal with three-dimensional rotations. Therefore, this method is not applicable for large rotations. Thus, he limited his approach to rotations to the range of 12–15 degrees. However, the formulation of the three-dimensional beam element is not just a simple extension of the two-dimensional formulation, mainly because of the complexity of the three-dimensional large rotations. More specifically, the three-dimensional large rotations are noncommutative and nonadditive. To handle this problem, Oran [24] used a joint orientation matrix to describe a set of orthogonal axes that are rigidly attached and deformed with the joints of a structure. The element nodal rotations are determined from the angles between this set of orthogonal axes and the member axes. This procedure is improved by Crisfield [25], Le et al. [26], Jonker and Meijaard [27], and Hsiao et al. [28]. Though this method does not put restriction on the size of the time step and can use smaller number of elements, a key stone for the method is the need for a special parametrization of the finite rotations. It also increases the computational time because of storing the joint orientation matrices and parametrization of the finite rotations. Bathe and Bolourchi [29] defined a moving local frame through three successive rotations similar to Euler angles, sometimes called Tait–Bryan angles, Bunge, or other conventions. However, they did not formulate trigonometric rules for all rotation angles. Benjamin [30] contributed to the solution of this problem by obtaining cosines and sins of all rotation's angles. However, he did not specify a control sign for the cosine of rotation angles which can be obtained using two hypotenuses of right-angle triangles. Nunes et al. [31] controlled the sign of the cosine of rotation angles to overcome the problem of the cosine of an angle greater than $\pi/2$. Nevertheless, they did not specify clearly how to determine the transformation matrices in the case of vertical members, when the rotation angle is equal $\pi/2$ or $-\pi/2$ exactly, which is very important in the modeling of three-dimensional structures. Furthermore, they did not solve any three-dimensional problem by examining their motion description method. Due to such problems, Simo and Vu-Quoc [16] identified the problem of singularity in case of using this method. That is why many authors used parametrization of finite rotations, such as the authors in [16, 25–27].

To express the stiffness and mass matrices, the Euler–Bernoulli beam theory was extensively used in the formulations by many researchers (see, for example, [21, 22, 27, 28, 32, 33]) since it simplified the analysis and in the same time obtains adequate results. In the Euler–Bernoulli beam theory, the material is considered isotropic and elastic, and the cross section of the elements is uniform. A normal plane section on the centroid axis before deformation remains plane after deformation and normal to the axis is employed. Warping and cross-sectional distortion are not considered. To investigate the effect of shear formulation, the Timoshenko beam model has been used by other researchers (see, for example, [15, 22, 34]).

In this paper, a relatively accurate and simple corotational formulation for three-dimensional finite element formulation has been developed. The stiffness and mass matrices are evaluated using the Euler–Bernoulli beam

model. The transformation procedure is based on the Tait–Bryan angles successive rotations [23, 29]. This procedure is employed in two main stages to transform vectors and matrices from the fixed global frame to the moving corotational frame. The first stage is the transformation from the fixed global frame to the fixed local frame, and the second stage is the transformation from the fixed local frame to the moving corotational local frame. The transformation procedure also depends upon updating the coordinates with every equilibrium configuration during the analysis. In order to formulate a consistent model, the trigonometric rules for special cases of spatial beam elements are considered with the control sign. These rules are used to calculate the rotations matrices. Meanwhile, this method is simple and does not need parametrization for finite rotations, but it requires regulating the time step and number of elements in order to decrease the relative chordal rotations during the analysis. The equation of motion is formulated using Lagrange's equation. An incremental iterative procedure is used to solve the equation of motion. This procedure is based on the full Newton–Raphson method and the Newmark direct-time integration method. The MATLAB code is developed for this purpose. This code involves a relatively rapid convergence rate for equilibrium because it avoids storing joint orientation matrices and parametrizing of finite rotations, which are often associated with parametrized formulations. This section represents a general introduction and reveals the importance of studying geometric nonlinearity. The spatial beam element motion description method, which involves the coordinate systems and the displacement interpolation, is presented in Section 2. The transformation procedure between different coordinate systems based on Tait–Bryan angles can be seen in Section 3. The strain energy and stiffness matrix are derived in Section 4. The kinetic energy and the mass matrix are presented in Section 5. Then, Lagrange's equation is used to derive the equation of motion in Section 6. Section 7 represents the solution strategy. To expose the efficiency and validate the accuracy of the proposed model, five numerical examples are solved and compared with the published results in Section 8. Finally, the conclusions are presented in Section 9.

2. Kinematics Description of the 3D Beam Element

2.1. Basic Assumptions. The following assumptions are employed to formulate the spatial beam element:

(i) The material is isotropic, elastic, and homogeneous

(ii) The cross section of the beam element is symmetric about both axes

(iii) Euler–Bernoulli beam assumptions, which state that a normal plane section on the centroid axis before deformation remains plane after deformation and is normal to that axis, are employed.

(iv) Warping, cross-sectional distortion, and shear effect are not taken into account

Hence, the small strain theory is the basis for the corotational formulation used in the analysis. Accordingly, deformational and rotational displacements are always small with respect to the corotational frame. Appropriate element sizes and time steps are chosen to ensure that these conditions remain valid and the results are accurate.

2.2. Coordinate Systems. After discretization of the structure into finite elements, the i^{th} beam element can be defined with two end nodes ($n = 1$ and 2). Every node has six degrees of freedom and is defined with respect to three frames as shown in Figure 1. These coordinate systems are the fixed global coordinate system associated with the fixed global frame (X, Y, Z), the fixed local coordinate system associated with the fixed local frame at time = 0 ($\hat{x}_i$, $\hat{y}_i$, $\hat{z}_i$), and the moving local coordinate system associated with the corotational local frame ($\overline{x}_i$, $\overline{y}_i$, $\overline{z}_i$). This local corotational frame is updated and attached to each beam element. It also translates and rotates with the beam element but does not deform with it. Figure 1 also shows the three configurations used in dynamics: an initial configuration at time = 0, the j^{th} equilibrium configuration at time = t, and a current configuration at time = $t + \Delta t$. The element's initial length is L_o, and after deformation in the current configuration, the element length is equal to the arc length S_i, while L_c is the current chord length.

For the current configuration, as shown in Figure 2, the nodal displacement vector for the i^{th} beam element in the fixed global coordinate system is given by the following equation:

$$\mathbf{D}_i = \left[U_1\, V_1\, W_1\, \theta X_1\, \theta Y_1\, \theta Z_1\, U_2\, V_2\, W_2\, \theta X_2\, \theta Y_2\, \theta Z_2\right]^T, \tag{1}$$

where U_n ($n = 1, 2$), V_n ($n = 1, 2$), and W_n ($n = 1, 2$) are the displacement translational components in X, Y, and Z directions, respectively, and θX_n. θY_n and θZ_n ($n = 1, 2$) are the counterclockwise rotations about X, Y, and$Z$ axes, respectively.

The nodal incremental displacement vector of the i^{th} beam element in the global coordinate system is defined as follows:

$$\Delta\mathbf{D}_i = \left[\Delta U_1\, \Delta V_1\, \Delta W_1\, \Delta\theta X_1\, \Delta\theta Y_1\, \Delta\theta Z_1\, \Delta U_2\, \Delta V_2\, \Delta W_2\, \Delta\theta X_2\, \Delta\theta Y_2\, \Delta\theta Z_2\right]^T, \tag{2}$$

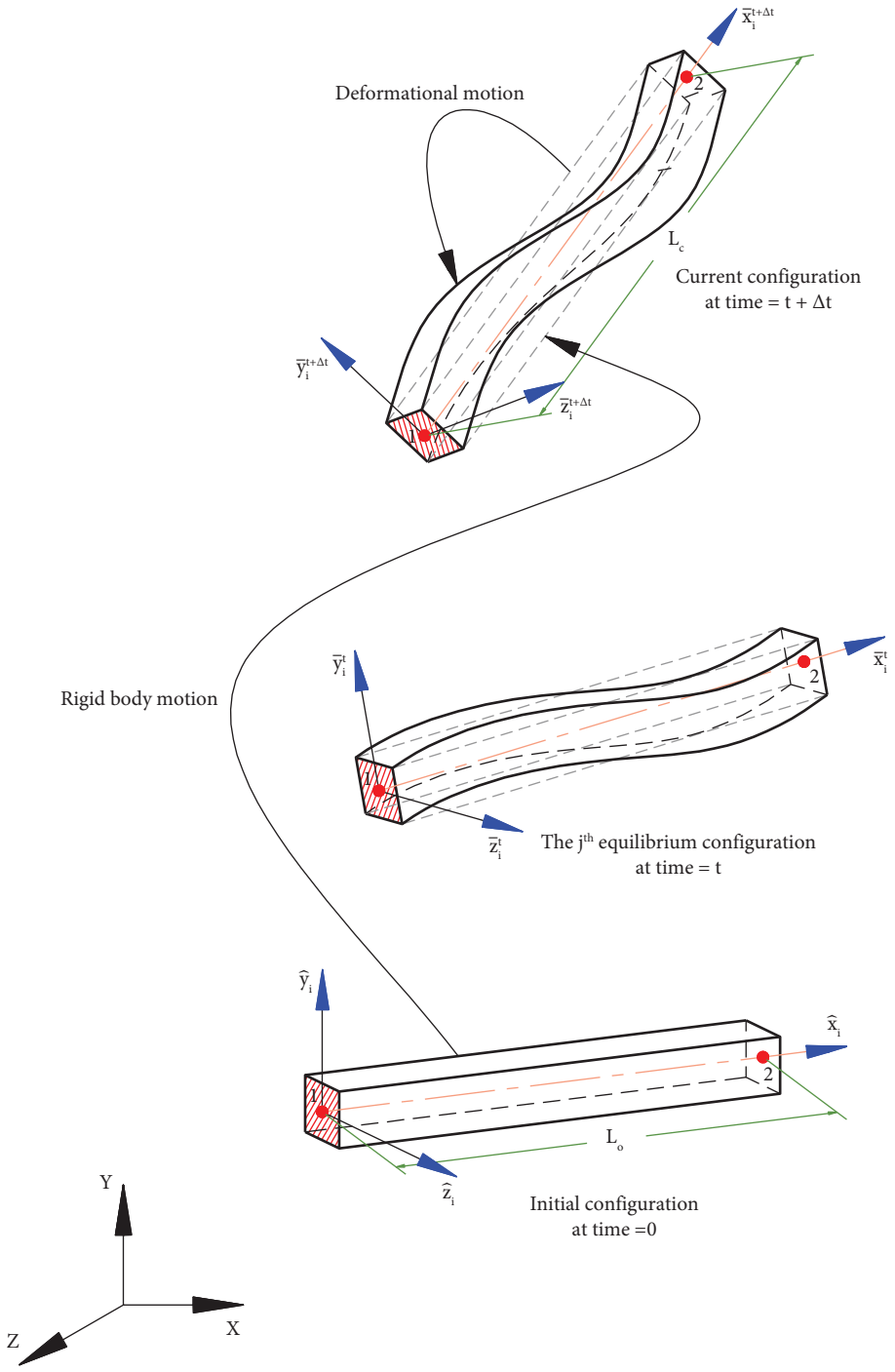

Figure 1: Motion and coordinate systems of the i^{th} spatial beam element.

where ΔU_n $(n = 1, 2)$, ΔV_n $(n = 1, 2)$, and ΔW_n $(n = 1, 2)$ are the incremental translational components of displacement in X, Y, and Z directions, respectively, and $\Delta\theta X_n$.$\Delta\theta Y_n$ and $\Delta\theta Z_n$ $(n = 1, 2)$ are the counterclockwise incremental rotations about X, Y, and Z axes, respectively. The nodal displacement vector $\mathbf{D}_i$ can be updated by the following equation:

$$\mathbf{D}_i = \mathbf{D}_i^j + \Delta\mathbf{D}_i, \tag{3}$$

where $\mathbf{D}_i^j$ is the nodal displacement vector for the i^{th} beam element in the fixed global coordinate system at the j^{th} equilibrium configuration. The nodal displacement vector $\mathbf{D}_i$ is divided into the nodal translational displacement

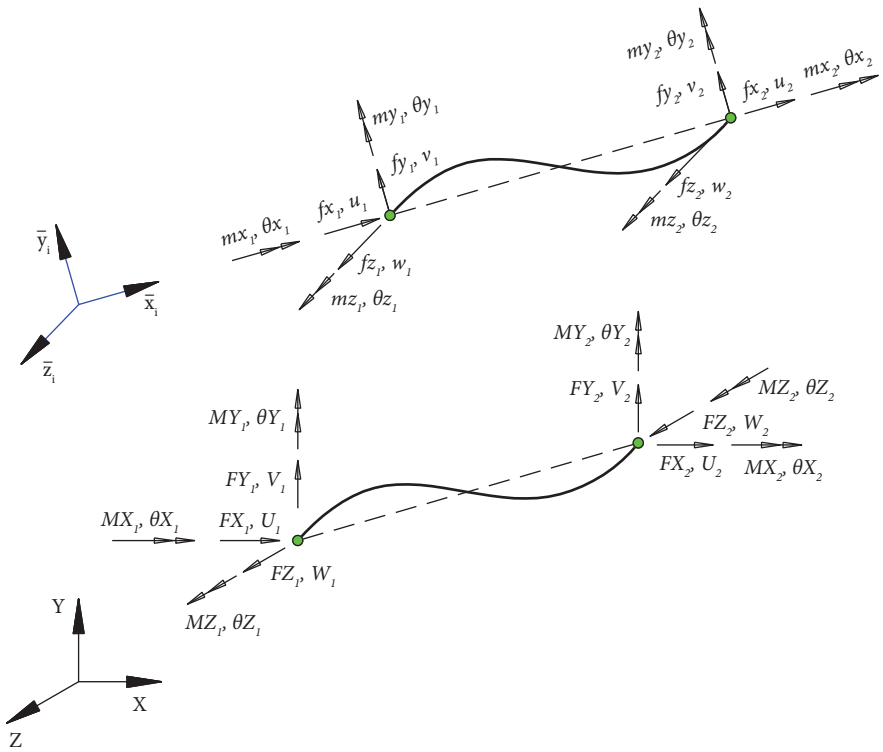

FIGURE 2: Displacement and force nodal components with positive signs of the i^{th} beam element in the global coordinate system and the corotational local coordinate system.

vector $\mathbf{Dt}_i$ and the nodal rotational displacement vector $\mathbf{Dr}_i$, which can be written as follows:

$$\begin{aligned}\mathbf{Dt}_i &= \left[U_1\, V_1\, W_1\, U_2\, V_2\, W_2\right]^T,\\ \mathbf{Dr}_i &= \left[\theta X_1\, \theta Y_1\, \theta Z_1\, \theta X_2\, \theta Y_2\, \theta Z_2\right]^T.\end{aligned} \tag{4}$$

Similarly, the $\Delta\mathbf{D}_i$ vector can be divided into the nodal incremental translational displacement vector $\Delta\mathbf{Dt}_i$ and the nodal incremental rotational displacement vector $\Delta\mathbf{Dr}_i$ as follows:

$$\Delta\mathbf{Dt}_i = \left[\Delta U_1\, \Delta V_1\, \Delta W_1\, \Delta U_2\, \Delta V_2\, \Delta W_2\right]^T, \tag{5}$$

$$\Delta\mathbf{Dr}_i = \left[\Delta\theta X_1\, \Delta\theta Y_1\, \Delta\theta Z_1\, \Delta\theta X_2\, \Delta\theta Y_2\, \Delta\theta Z_2\right]^T. \tag{6}$$

Thus, the nodal coordinate vector of the i^{th} beam element in the fixed global system can be updated continuously as follows:

$$\begin{aligned}\mathbf{X}_i &= \mathbf{X}_n^j + \Delta\mathbf{Dt}_i,\\ \mathbf{X}_i &= \left[\, X_i \;\; Y_i \;\; Z_i\right]^T,\end{aligned} \tag{7}$$

where $\mathbf{X}_i$ is the vector of the nodal coordinates of the i^{th} beam element relative to the fixed global frame, at the current configuration, and $\mathbf{X}_i^j$ is the vector of the nodal coordinates relative to the fixed global frame, at the j^{th} equilibrium configuration.

The nodal displacement vector of the i^{th} beam element in the element corotational local coordinate system, at the current configuration, is as follows:

$$\mathbf{d}_{\text{i}} = \left[u_1\, v_1\, w_1\, \theta x_1\, \theta y_1\, \theta z_1\, u_2\, v_2\, w_2\, \theta x_2\, \theta y_2\, \theta z_2\right]^T, \tag{8}$$

where u_n (n = 1, 2), v_n (n = 1, 2), and w_n (n = 1, 2) are the displacement translational components in $\overline{x}_i$, $\overline{y}_i$, and $\overline{z}_i$ directions, respectively, and θx_n. θy_n. and θz_n (n = 1 and 2) are the counterclockwise deformational rotations after eliminating the rigid-body rotations.

The internal elastic force vector for the i^{th} beam element in the fixed global coordinate system, at the current configuration, can be written as follows:

$$\mathbf{F}_{\text{i}}^{\text{e}} = \left[FX_1\, FY_1\, FZ_1\, MX_1\, MY_1\, MZ_1\, FX_2\, FY_2\, FZ_2\, MX_2\, MY_2\, MZ_2\right]^T. \tag{9}$$

The internal elastic force vector of the i^{th} beam element in the element corotational local coordinate system, at the current configuration, is as follows:

$$\mathbf{f_i^e} = \left[fx_1\ fy_1\ fz_1\ mx_1\ my_1\ mz_1\ fx_2\ fy_2\ fz_2\ mx_2\ my_2\ mz_2\right]^T, \tag{10}$$

where the internal elastic force vector components in both the fixed global coordinate system and the corotational local coordinate system are shown in Figure 2 with their positive signs.

2.3. Displacement Interpolation. The classical Hermitian shape functions are used to relate the element axial elongation $u(\overline{x}_i)$, lateral deflections of the centroid axis $v(\overline{x}_i)$ and $w(\overline{x}_i)$ shown in Figure 3, and rotation about the centroid axis $\theta_x(\overline{x}_i)$ to the element nodal displacement vector $\mathbf{d}_i$ as follows:

$$u(\overline{x}_i) = \begin{bmatrix} N_1 & 0 & 0 & 0 & 0 & 0 & N_4 & 0 & 0 & 0 & 0 & 0 \end{bmatrix}\mathbf{d}_i, \tag{11}$$

$$v(\overline{x}_i) = \begin{bmatrix} 0 & N_2 & 0 & 0 & 0 & N_3 & 0 & N_5 & 0 & 0 & 0 & N_6 \end{bmatrix}\mathbf{d}_i, \tag{12}$$

$$w(\overline{x}_i) = \begin{bmatrix} 0 & 0 & N_2 & 0 & -N_3 & 0 & 0 & 0 & N_5 & 0 & -N_6 & 0 \end{bmatrix}\mathbf{d}_i, \tag{13}$$

$$\theta_x(\overline{x}_i) = \begin{bmatrix} 0 & 0 & 0 & N_1 & 0 & 0 & 0 & 0 & 0 & N_4 & 0 & 0 \end{bmatrix}\mathbf{d}_i. \tag{14}$$

The components of the shape functions $\mathbf{N}_i$ of the i^{th} beam element are given by the following equation:

$$\begin{aligned} N_1 &= 1 - \frac{1}{2}(1+\xi), \\ N_2 &= \frac{1}{4}(1-\xi)^2(2+\xi), \\ N_3 &= \frac{L_c}{8}\left(1-\xi^2\right)(1-\xi), \\ N_4 &= \frac{1}{2}(1+\xi), \\ N_5 &= \frac{1}{4}(1+\xi)^2(2-\xi), \\ N_6 &= \frac{L_c}{8}\left(-1+\xi^2\right)(1+\xi), \end{aligned} \tag{15}$$

where ξ is given by

$$\xi = -1 + \frac{2\overline{x}_i}{L_c}, \tag{16}$$

where L_c is the element current chord length.

The function ξ nodal values for the i^{th} beam element are shown in Figure 4. Transverse displacements can be determined, at any point along the element, using shape functions and the nodal displacement values in the local coordinate system.

Due to the nature of the attached corotational local frame, as shown in Figures 1 and 3, the displacement components v_n $(n = 1,2)$ and w_n $(n = 1,2)$ are equal to zero. Furthermore, the axial displacement of the first node is chosen to be zero while the axial displacement of the second node is u_2. Consequently, the nodal displacement vector $\mathbf{d}_i$ has only seven nonzero components which will simplify the analysis as can be seen in the next section. This vector can be written as follows:

$$\mathbf{d}_i = \begin{bmatrix} 0 & 0 & 0 & \theta x_1 & \theta y_1 & \theta z_1 & u_2 & 0 & 0 & \theta x_2 & \theta y_2 & \theta z_2 \end{bmatrix}^T. \tag{17}$$

Thus, equations (12) and (13) can be simplified to

$$\begin{aligned} v(\overline{x}_i) &= N_3\,\theta z_1 + N_6\,\theta z_2, \\ w(\overline{x}_i) &= -N_3\,\theta y_1 - N_6\,\theta y_2. \end{aligned} \tag{18}$$

The arc length of the i^{th} beam element S_i can be expressed by

$$S_i = \frac{L_c}{2}\int_{-1}^{1}\sqrt{\left(v'^2 + w'^2 + 1\right)}\,\mathrm{d}\xi, \tag{19}$$

where v' and w' are the first derivatives of the functions $v(\overline{x}_i)$ and $w(\overline{x}_i)$ with respect to $\overline{x}_i$. This integral is evaluated using the Gaussian integration scheme. The axial elongation of the i^{th} beam element can be defined as follows:

$$e = S_i - L_o. \tag{20}$$

This equation can also be written in terms of chord lengths as follows:

$$e = L_c - L_o + b_i, \tag{21}$$

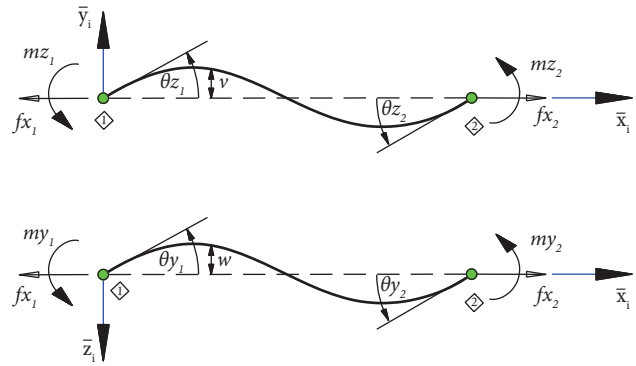

Figure 3: The i^{th} beam element displacement and internal force vector components with the attached corotational local frame in planes $(\bar{x}_i - \bar{y}_i)$ and $(\bar{x}_i - \bar{z}_i)$.

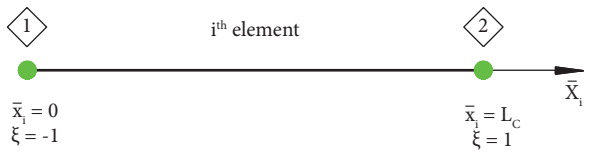

Figure 4: The values of ξ function along the i^{th} beam element end nodes.

where L_o is the element initial length and b_i is the element axial elongation due to the bowing effect, which can be determined in terms of rotations [35] as follows:

$$b = \frac{L_c}{30}\left[2\theta y_1^2 - \theta y_1 \theta y_2 + 2\theta y_2^2\right] + \frac{L_c}{30}\left[2\theta z_1^2 - \theta z_1 \theta z_2 + 2\theta z_2^2\right]. \tag{22}$$

Hence, the axial displacement u_2 in equation (17) is given by

$$u_2 = e. \tag{23}$$

3. Transformation Procedure

The transformation procedure depends upon updating the coordinates with every equilibrium configuration during the analysis. Two main stages are employed here to perform transformation from the fixed global frame to the moving corotational local frame. The first stage is the transformation from the fixed global frame to the fixed local frame, and the second stage is the transformation from the fixed local frame to the moving corotational local frame.

Assuming that $\mathbf{V}_d$ is a 3D vector associated with the fixed global frame, the relation between the fixed global frame (X, Y, Z) and the fixed local frame $(\hat{x}_i, \hat{y}_i, \hat{z}_i)$ can be expressed by the following equation:

$$\hat{\mathbf{v}}_d = \mathbf{r}_o \mathbf{V}_d, \tag{24}$$

where $\mathbf{r}_o$ is an orthogonal matrix (3×3) which can be determined from the direction cosines of the fixed local frame relative to the fixed global frame. For a three-dimensional frame element, this matrix turns into a (12×12) matrix as follows:

$$\mathbf{T}_o = \begin{bmatrix} \mathbf{r}_o & \mathbf{0} & \mathbf{0} & \mathbf{0} \\ \mathbf{0} & \mathbf{r}_o & \mathbf{0} & \mathbf{0} \\ \mathbf{0} & \mathbf{0} & \mathbf{r}_o & \mathbf{0} \\ \mathbf{0} & \mathbf{0} & \mathbf{0} & \mathbf{r}_o \end{bmatrix}. \tag{25}$$

Similarly, the relation between the fixed local frame $(\hat{x}_i, \hat{y}_i, \hat{z}_i)$ and the current corotational local frame $(\bar{x}_i, \bar{y}_i, \bar{z}_i)$ is

$$\bar{\mathbf{v}}_d = \mathbf{r}_c \hat{\mathbf{v}}_d, \tag{26}$$

where $\mathbf{r}_c$ is also an orthogonal matrix (3×3) which can be obtained from the direction cosines of the corotational local frame relative to the fixed local frame. For a three-dimensional frame element, this matrix turns into a (12×12) matrix as follows:

$$\mathbf{T}_c = \begin{bmatrix} \mathbf{r}_c & \mathbf{0} & \mathbf{0} & \mathbf{0} \\ \mathbf{0} & \mathbf{r}_c & \mathbf{0} & \mathbf{0} \\ \mathbf{0} & \mathbf{0} & \mathbf{r}_c & \mathbf{0} \\ \mathbf{0} & \mathbf{0} & \mathbf{0} & \mathbf{r}_c \end{bmatrix}. \tag{27}$$

One can write the vector $\bar{\mathbf{v}}_d$ in terms of $\mathbf{V}_d$ as follows:

$$\bar{\mathbf{v}}_d = \mathbf{r}_r \mathbf{V}_d, \tag{28}$$

where

$$\mathbf{r}_r = \mathbf{r}_c \mathbf{r}_o. \tag{29}$$

Therefore, the transformation matrix for the three-dimensional i^{th} beam element from the fixed global frame to the moving corotational local frame, at the current configuration, can be expressed by

$$\mathbf{T}_r = \mathbf{T}_c \mathbf{T}_o. \tag{30}$$

Both transformation matrices $\mathbf{r}_o$ and $\mathbf{r}_c$ are determined using Tait–Bryan angles, which describe the three successive rotations of the three-dimensional beam element.

3.1. Transformation from the Fixed Global Frame to the Fixed Local Frame. The first stage is to transform from the fixed global system to the fixed local system using the three successive rotations β_o, γ_o, α_o, as shown in Figures 5–8, as follows:

(1) Rotation β_o of the (X, Y, Z) coordinate axes about the Y axis: This rotation places the X and Z axis along X_{β_o} and Z_{β_o}, respectively, while the Y axis remains the same, as shown in Figure 5.

Using the direction cosines of β_o frame $(X_{\beta_o}, Y, Z_{\beta_o})$ with respect to the global frame (X, Y, Z), shown in Figures 5 and 8, the rotation matrix $\mathbf{r}_{\beta_o}$ can be determined as follows:

$$\mathbf{r}_{\beta_o} = \begin{bmatrix} \cos\beta_o & 0 & \sin\beta_o \\ 0 & 1 & 0 \\ -\sin\beta_o & 0 & \cos\beta_o \end{bmatrix}, \tag{31}$$

where

$$\cos\beta_o = \frac{C_X}{C_{XZ}},$$

$$\sin\beta_o = \frac{C_Z}{C_{XZ}},$$

$$C_X = \frac{X_2 - X_1}{L_o},$$

$$C_Y = \frac{Y_2 - Y_1}{L_o},$$

$$C_Z = \frac{Z_2 - Z_1}{L_o},$$

$$C_{XZ} = \sqrt{C_X{}^2 + C_Z{}^2},$$

$$L_o = \sqrt{(X_2 - X_1)^2 + (Y_2 - Y_1)^2 + (Z_2 - Z_1)^2}. \tag{32}$$

(2) Rotation γ_o of the $(X_{\beta_o}, Y, Z_{\beta_o})$ coordinate axes about the Z_{β_o} axis: This rotation places the X_{β_o} and Y axis along X_{γ_o} and Y_{γ_o}, respectively, while the Z_{β_o} axis remains the same, as shown in Figure 6. One can use the direction cosines of the γ_o frame $(X_{\gamma_o}, Y_{\gamma_o}, Z_{\beta_o})$ with respect to the β_o frame $(X_{\beta_o}, Y, Z_{\beta_o})$, and the rotation matrix $\mathbf{r}_{\gamma_o}$ can be obtained as follows:

$$\mathbf{r}_{\gamma_o} = \begin{bmatrix} \cos\gamma_o & \sin\gamma_o & 0 \\ -\sin\gamma_o & \cos\gamma_o & 0 \\ 0 & 0 & 1 \end{bmatrix}, \tag{33}$$

where

$$\cos\gamma_o = C_{XZ},$$
$$\sin\gamma_o = C_Y. \tag{34}$$

(3) Rotation α_o of the $(X_{\gamma_o}, Y_{\gamma_o}, Z_{\beta_o})$ coordinate axes about X_{γ_o} axis: This rotation places the Y_{γ_o} and Z_{γ_o} axis along $\hat{y}_i$ and $\hat{z}_i$, respectively, while the X_{γ_o} axis remains the same. It has to be noticed that $\hat{x}_i$ coincides with the axis X_{γ_o}, as shown in Figure 7.

By assuming a point P lies in the $(\hat{x}_i, \hat{y}_i)$ plane, as shown in Figure 8, the point P coordinates relative to the starting point of the i^{th} beam element with respect to the fixed global system coordinate (X, Y, Z) can be written as follows:

$$X_{P1} = X_P - X_1,$$
$$Y_{P1} = Y_P - Y_1, \tag{35}$$
$$Z_{P1} = Z_P - Z_1.$$

Consequently, the coordinates of point P with respect to the $(X_{\gamma_o}, Y_{\gamma_o}, Z_{\gamma_o})$ frame, as shown in Figure 9, can be obtained as follows:

$$\begin{bmatrix} X_{P\gamma_o} & Y_{P\gamma_o} & Z_{P\gamma_o} \end{bmatrix}^T = \mathbf{r}_{\gamma_o}\mathbf{r}_{\beta_o}\begin{bmatrix} X_{P1} & Y_{P1} & Z_{P1} \end{bmatrix}^T, \tag{36}$$

which leads to

$$X_{P\gamma_o} = C_X X_{P1} + C_Y Y_{P1} + C_Z Z_{P1},$$
$$Y_{P\gamma_o} = -\frac{C_X C_Y}{C_{XZ}} X_{P1} + C_{XZ} Y_{P1} - \frac{C_Y C_Z}{C_{XZ}} Z_{P1}, \tag{37}$$
$$Z_{P\gamma_o} = -\frac{C_Z}{C_{XZ}} X_{P1} + \frac{C_X}{C_{XZ}} Z_{P1}.$$

Now, using the direction cosines of α_o frame $(X_{\alpha_o}, Y_{\alpha_o}, Z_{\alpha_o})$, which coincides with the $(\hat{x}_i, \hat{y}_i, \hat{z}_i)$ frame, with respect to previous frame $(X_{\gamma_o}, Y_{\gamma_o}, Z_{\gamma_o})$, the rotation matrix $\mathbf{r}_{\alpha_o}$ can be determined as follows:

$$\mathbf{r}_{\alpha_o} = \begin{bmatrix} 1 & 0 & 0 \\ 0 & \cos\alpha_o & \sin\alpha_o \\ 0 & -\sin\alpha_o & \cos\alpha_o \end{bmatrix}, \tag{38}$$

where

$$\cos\alpha_o = \frac{Y_{P\gamma_o}}{\sqrt{\left(Y_{P\gamma_o}\right)^2 + \left(Z_{P\gamma_o}\right)^2}}, \tag{39}$$

$$\sin\alpha_o = \frac{Z_{P\gamma_o}}{\sqrt{\left(Y_{P\gamma_o}\right)^2 + \left(Z_{P\gamma_o}\right)^2}}. \tag{40}$$

Hence, the rotation matrix $\mathbf{r}_o$ can be obtained as follows:

$$\mathbf{r}_o = \mathbf{r}_{\alpha_o}\mathbf{r}_{\gamma_o}\mathbf{r}_{\beta_o}. \tag{41}$$

By substitution, this matrix takes the form as follows:

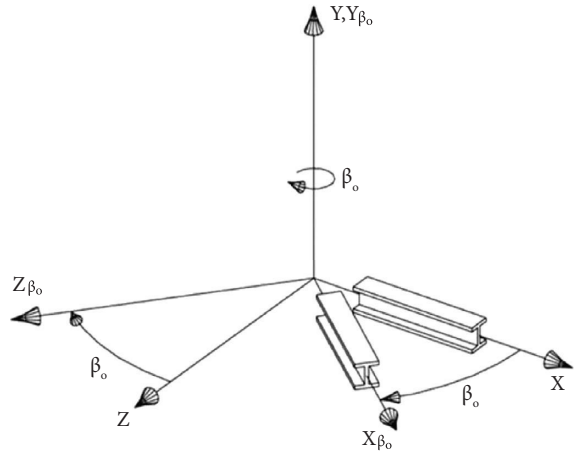

Figure 5: Rotation angle β_o of coordinate axes about Y axis (X, Y, X) to (X_{β_o}, Y, Z_{β_o}).

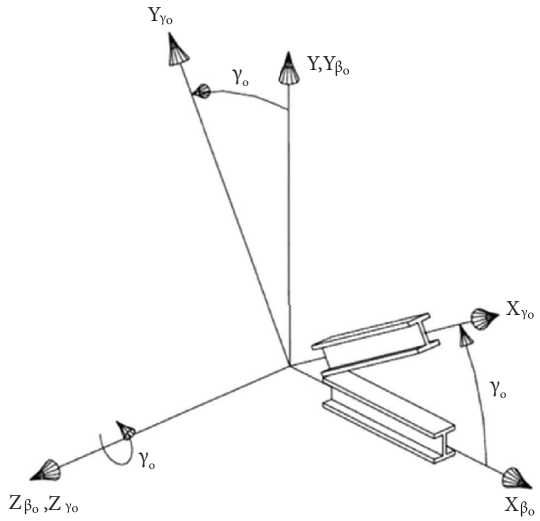

Figure 6: Rotation angle γ_o of coordinate axes about Z_{β_o} axis (X_{β_o}, Y, Z_{β_o}) to (X_{γ_o}, Y_{γ_o}, Z_{β_o}).

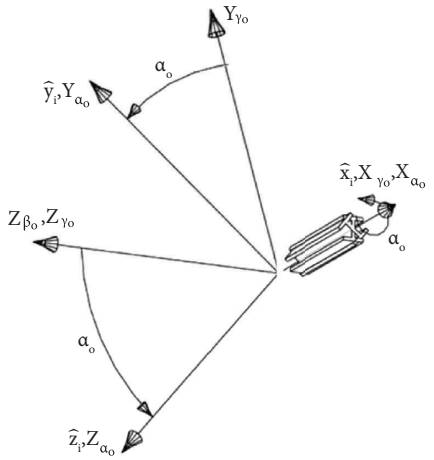

Figure 7: Rotation angle α_o of coordinate axes about X_{γ_o} axis (X_{γ_o}, Y_{γ_o}, Z_{β_o}) to ($\hat{x}_i$, $\hat{y}_i$, $\hat{z}_i$).

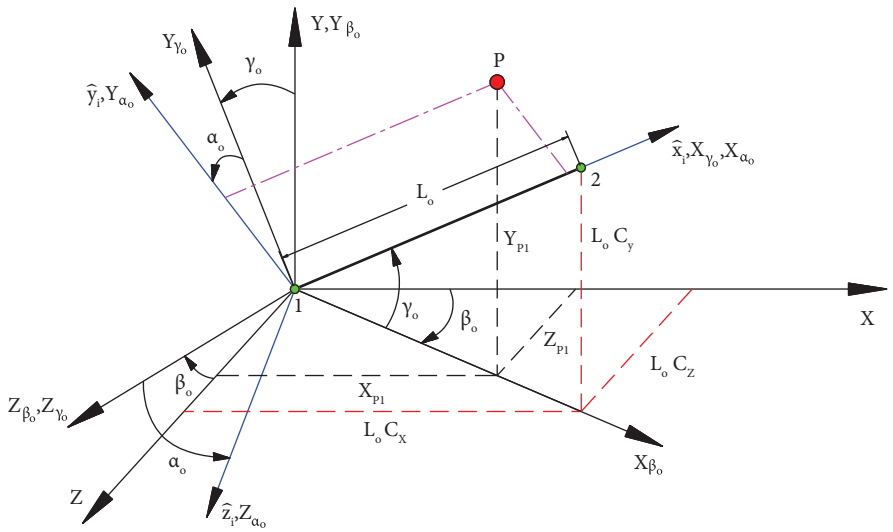

Figure 8: Three successive rotations (β_o, γ_o, α_o) of a three-dimensional beam element.

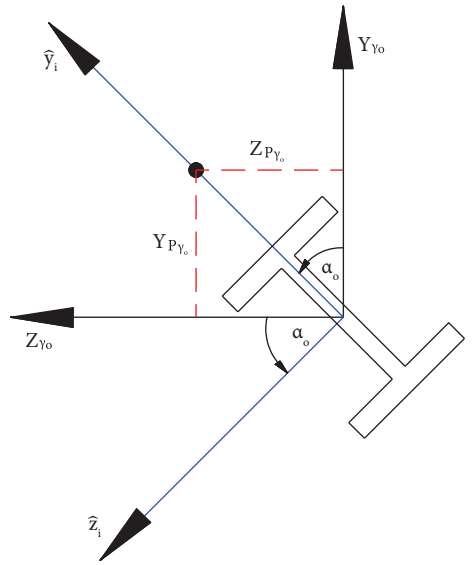

Figure 9: The reference point (P) coordinates relative to the frame (X_{γ_o}, Y_{γ_o}, Z_{γ_o}).

$$\mathbf{r}_o = \begin{bmatrix} C_X & C_Y & C_Z \\ \dfrac{-C_X C_Y \cos\alpha_o - C_Z \sin\alpha_o}{C_{XZ}} & C_{XZ}\cos\alpha_o & \dfrac{-C_Y C_Z \cos\alpha_o + C_X \sin\alpha_o}{C_{XZ}} \\ \dfrac{C_X C_Y \sin\alpha_o - C_Z \cos\alpha_o}{C_{XZ}} & -C_{XZ}\sin\alpha_o & \dfrac{C_Y C_Z \sin\alpha_o + C_X \cos\alpha_o}{C_{XZ}} \end{bmatrix}. \tag{42}$$

3.1.1. Special Cases. It should be noted that the rotation angle α_o is insignificant, in the case of a circular cross section element. Thus, the rotation matrix $\mathbf{r}_o$ can be calculated as follows:

$$\mathbf{r}_o = \mathbf{r}_{\gamma_o}\mathbf{r}_{\beta_o}. \tag{43}$$

There is another special case where the initial position of the element is vertical, in the Y-axis direction. In order to get $\mathbf{r}_o$, there are only two successive rotations not three as in the general case. The first rotation γ_o is either 90° or 270°, as shown in Figure 10, depending on whether C_Y is +1 or −1. The other rotation is α_o, which is shown in Figure 11, and

can be determined using a reference the point P that lies in the $(\hat{x}_i, \hat{y}_i)$ plane. In this case, equations (39) and (40) are modified as follows:

$$\cos\alpha_o = -\frac{X_{P1}}{\sqrt{(X_{P1})^2 + (Z_{P1})^2}}(C_Y),$$
$$\sin\alpha_o = \frac{Z_{P1}}{\sqrt{(X_{P1})^2 + (Z_{P1})^2}}. \tag{44}$$

Thus, the matrix $\mathbf{r}_o$ in equation (43) can be written as follows:

$$\mathbf{r}_o = \begin{bmatrix} 0 & C_Y & 0 \\ -C_Y\cos\alpha_o & 0 & \sin\alpha_o \\ C_Y\sin\alpha_o & 0 & \cos\alpha_o \end{bmatrix}. \tag{45}$$

Substituting equation (42) or equation (45) into equation (25), the matrix $\mathbf{T}_o$ can be determined.

3.2. Transformation from the Fixed Local Frame to the Moving Corotational Local Frame. The second stage is to transform from the fixed local system $(\hat{x}_i, \hat{y}_i, \hat{z}_i)$ to the moving corotational local system $(\overline{x}_i, \overline{y}_i, \overline{z}_i)$, at the current configuration, using the three successive rotations β_c, γ_c, and α_c, as shown in Figure 12. These rotations are similar to the rotations β_o, γ_o, and α_o in Figures 5–7; however, the calculation method depends upon the relative displacements.

(1) Using the direction cosines of the β_c frame $(X_{\beta_c}, Y_{\beta_c}, Z_{\beta_c})$ with respect to fixed local frame $(\hat{x}_i, \hat{y}_i, \hat{z}_i)$, which is shown in Figure 12, the rotation matrix $\mathbf{r}_{\beta_c}$ can be determined as follows:

$$\mathbf{r}_{\beta_c} = \begin{bmatrix} \cos\beta_c & 0 & \sin\beta_c \\ 0 & 1 & 0 \\ -\sin\beta_c & 0 & \cos\beta_c \end{bmatrix}, \tag{46}$$

where

$$\cos\beta_c = \frac{\mathrm{L_o} + \hat{U}_i^r}{\overline{P_1P_2'}},$$
$$\sin\beta_c = \frac{\hat{W}_i^r}{\overline{P_1P_2'}} \tag{47}$$
$$\overline{P_1P_2'} = \sqrt{\left(L_o + \hat{U}_i^r\right)^2 + \left(\hat{W}_i^r\right)^2}.$$

Of particular interest is to notice that in [29], a difficulty arises when angle $\beta_c > 90^\circ$ since this reference gave only an expression of the cosine of the angle. In this work, an expression for sine is also given. Both trigonometric relations can specify the location of the element exactly. As shown in Figure 12, $\hat{U}_i^r$, $\hat{V}_i^r$, and $\hat{W}_i^r$ are the i^{th} beam element relative translational displacements with respect to the fixed local frame. These relative displacements of the i^{th} beam element can be determined from the relative displacement with respect to the fixed global system calculated from the $\mathbf{Dt}_i$ vector in equation (4) and the transformation matrix $\mathbf{r}_o$ in equation (41) or equation (43) for the vertical member as follows:

$$\begin{bmatrix} \hat{U}_i^r & \hat{V}_i^r & \hat{W}_i^r \end{bmatrix} = \begin{bmatrix} -\mathbf{r}_o & \mathbf{r}_o \end{bmatrix}\mathbf{Dt}_i, \tag{48}$$

where

$$\hat{U}_i^r = \mathbf{r}_{o_{(1,1)}}(U_2 - U_1) + \mathbf{r}_{o_{(1,2)}}(V_2 - V_1) + \mathbf{r}_{o_{(1,3)}}(W_2 - W_1), \tag{49}$$

$$\hat{V}_i^r = \mathbf{r}_{o_{(2,1)}}(U_2 - U_1) + \mathbf{r}_{o_{(2,2)}}(V_2 - V_1) + \mathbf{r}_{o_{(2,3)}}(W_2 - W_1), \tag{50}$$

$$\hat{W}_i^r = \mathbf{r}_{o_{(3,1)}}(U_2 - U_1) + \mathbf{r}_{o_{(3,2)}}(V_2 - V_1) + \mathbf{r}_{o_{(3,3)}}(W_2 - W_1). \tag{51}$$

(2) Similarly, one can use the direction cosines of the γ_c frame $(X_{\gamma_c}, Y_{\gamma_c}, Z_{\gamma_c})$ with respect to frame $(X_{\beta_c}, Y_{\beta_c}, Z_{\beta_c})$, and the rotation matrix $\mathbf{r}_{\gamma_c}$ can be obtained as follows:

$$\mathbf{r}_{\gamma_c} = \begin{bmatrix} \cos\gamma_c & \sin\gamma_c & 0 \\ -\sin\gamma_c & \cos\gamma_c & 0 \\ 0 & 0 & 1 \end{bmatrix}. \tag{52}$$

When employing the technique outlined in [29], a complication rises when the angle $\gamma_c > 90^\circ$, as this reference solely provides an expression for the sine of the angle. In this study, however, we present an expression for the cosine as well, enabling precise determination of the element's position. These two trigonometric relationships can be expressed as follows:

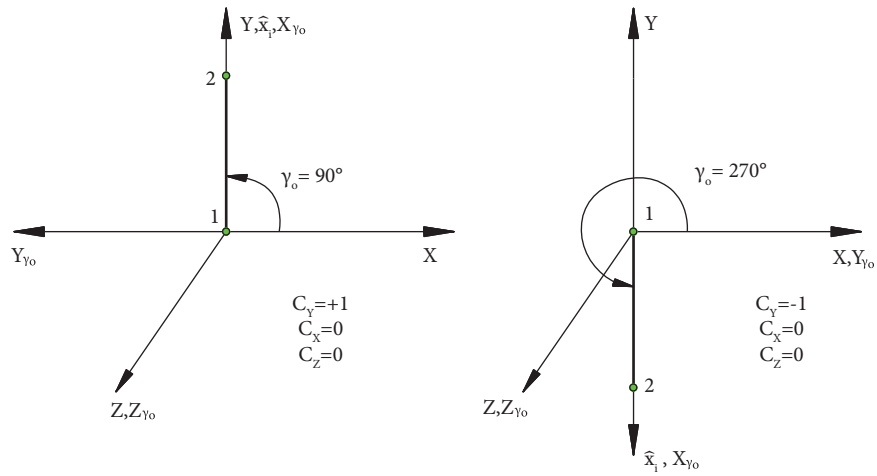

Figure 10: Vertical member cases and the rotation angle γ_o.

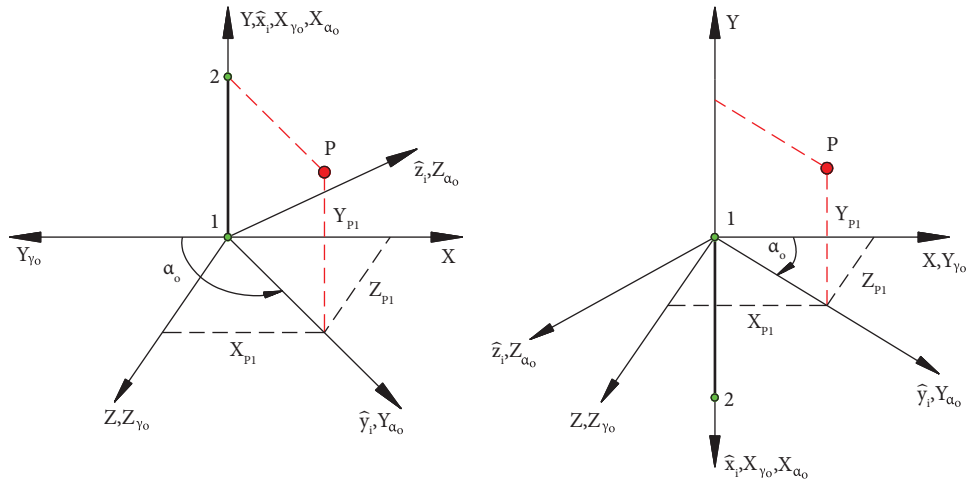

Figure 11: Vertical member cases and the rotation angle α_o with the reference point.

$$\cos\gamma_c = (\mathrm{SN})\frac{\overline{P_1P_2'}}{L_c}, \tag{53}$$

$$\sin\gamma_c = \frac{\hat{V}{}_i^r}{L_c}, \tag{54}$$

where

$$L_c = \sqrt{\left(\overline{P_1P_2'}\right)^2 + \left(\hat{V}{}_i^r\right)^2}, \tag{55}$$

and SN is equal +1 if $(L_o + \hat{U}{}_i^r) \geq 0$ and −1 if $(L_o + \hat{U}{}_i^r) < 0$.

The rotation matrix for relative translational displacements can be written as follows:

$$\mathbf{r}_{d_c} = \mathbf{r}_{\gamma_c}\,\mathbf{r}_{\beta_c}, \tag{56}$$

$$\mathbf{r}_{d_c} = \begin{bmatrix} \cos\beta_c\cos\gamma_c & \sin\gamma_c & \sin\beta_c\cos\gamma_c \\ -\cos\beta_c\sin\gamma_c & \cos\gamma_c & -\sin\beta_c\sin\gamma_c \\ -\sin\beta_c & 0 & \cos\beta_c \end{bmatrix}. \tag{57}$$

In case when an element becomes vertical, that means it is parallel to the Y-axis, the rotation β_c vanishes, and the rotation γ_c is either 90° or 270°, depending on the element position. Traditionally, this case could create singularity and it had been the source of many difficulties [31], and the authors of this research work suggested preventing the rotation γ_c to be either 90° or 270°. In this work, this problem is solved by letting the code search for the alignment of the element, that means to specify if the rotation γ_c is either 90° or 270°. The matrix $\mathbf{r}_{d_c}$ can be rewritten as follows:

$$\mathbf{r}_{d_c} = \begin{bmatrix} 0 & C_Y^{'} & 0 \\ -C_Y^{'} & 0 & 0 \\ 0 & 0 & 1 \end{bmatrix}, \tag{58}$$

where $C_Y^{'}$ can be specified using the current vector of the nodal coordinates in equation (7) as follows:

$$C_Y^{'} = \frac{Y_2 - Y_1}{L_c}. \tag{59}$$

Hence, the value of $C_Y^{'}$ is either +1 and the rotation γ_c is 90° or −1 and the rotation γ_c is 270°.

(3) When the third rotation angle α_c is computed by assuming a reference point P as has been done for α_o, it is very hard to assume a point in the $(\overline{x}_i, \overline{y}_i)$ plane every iteration with different consequence positions and directions. Accordingly, the model experienced some difficulties in converging using this method. Thus, an incremental procedure [29] is employed here to compute this angle as follows:

$$\Delta\alpha_c = \frac{1}{2}\left(\Delta\theta x_1 + \Delta\theta x_2\right), \tag{60}$$

where $\Delta\theta x_1$ and $\Delta\theta x_2$ are the incremental twist angles about the $\overline{x}_i$ axis. These incremental angles can be determined using the following procedure. First, the incremental rotational displacement vector, with respect to the fixed global frame in equation (6), is transformed to the corresponding vector in the fixed local frame using the procedure indicated in equation (24) as follows:

$$\left[\Delta\hat{\theta}x_n\, \Delta\hat{\theta}y_n\, \Delta\hat{\theta}z_n\right]^T = \mathbf{r}_o\left[\Delta\theta X_n\, \Delta\theta Y_n\, \Delta\theta Z_n\right]^T. \tag{61}$$

Then, the incremental rotational vector relative to the fixed local frame is transformed to the corotational local frame as follows:

$$\left[\Delta\theta x_n\, \Delta\theta y_n\, \Delta\theta z_n\right]^T = \mathbf{r}_{d_c}\left[\Delta\hat{\theta}x_n\, \Delta\hat{\theta}y_n\, \Delta\hat{\theta}z_n\right]^T. \tag{62}$$

Therefore, $\Delta\alpha_c$ in equation (60) can be determined using the following relation:

$$\Delta\alpha_c = \frac{1}{2}\left(\cos\beta_c \cos\gamma_c\left(\Delta\hat{\theta}x_1 + \Delta\hat{\theta}x_2\right) + \sin\gamma_c\left(\Delta\hat{\theta}y_1 + \Delta\hat{\theta}y_2\right) + \sin\beta_c \cos\gamma_c\left(\Delta\hat{\theta}z_1 + \Delta\hat{\theta}z_2\right)\right). \tag{63}$$

Consequently, the angle α_c, at the current configuration, can be determined as follows:

$$\alpha_c = \alpha_c^j + \Delta\alpha_c, \tag{64}$$

where α_c^j is the twist rotation about the $\overline{x}_i$ axis, at the j^{th} equilibrium configuration. This equation is used as a predictor between two successive time steps. Also, it is used as a corrector between two successive iterations.

Thus, the rotation matrix $\mathbf{r}_{\alpha_c}$ can be determined as follows:

$$\mathbf{r}_{\alpha_c} = \begin{bmatrix} 1 & 0 & 0 \\ 0 & \cos\alpha_c & \sin\alpha_c \\ 0 & -\sin\alpha_c & \cos\alpha_c \end{bmatrix}. \tag{65}$$

The rotation matrix $\mathbf{r}_c$ in equation (27) can be expressed as follows:

$$\mathbf{r}_c = \mathbf{r}_{\alpha_c}\, \mathbf{r}_{d_c}. \tag{66}$$

Substituting equations (65) and (57) (or equation (58) in case of vertical member) into equation (66), the matrix $\mathbf{r}_c$ can be determined. Hence, the transformation matrix $\mathbf{T}_c$ in equation (27) has been specified. Then, the transformation matrix $\mathbf{T}_r$ in equation (30) has been determined.

4. Strain Energy and the Stiffness Matrix

Considering isotropic elastic materials, the constitutive relation between the stress vector σ_i and the strain vector ϵ_i of the i^{th} beam element can be defined by the following equation:

$$\sigma_i = \mathbf{E}_i\, \epsilon_i, \tag{67}$$

where $\mathbf{E}_i$ is the symmetric matrix of the elastic coefficients. The strain vector is given by the following equation:

$$\epsilon_i = \mathbf{D}_f\, \mathbf{v_q}, \tag{68}$$

where $\mathbf{D}_f$ is the differential operator matrix and $\mathbf{v_q}$ is the deformation vector, which can be defined using the shape functions in equation (15) as follows:

$$\mathbf{v_q} = \mathbf{N}_i\, \mathbf{d}_i, \tag{69}$$

where $\mathbf{N}_i$ is the shape functions matrix, which is given in Appendix A.1. Substituting equation (69) into equation (68), the strain vector can be expressed as follows:

$$\epsilon_{\text{i}} = \mathbf{D}_f\, \mathbf{N}_i\, \mathbf{d}_i. \tag{70}$$

Combining equations (67) and (70), the stress vector can be rewritten as follows:

$$\boldsymbol{\sigma}_i = \mathbf{E}_i\, \mathbf{D}_f\, \mathbf{N}_i\, \mathbf{d}_i. \tag{71}$$

The strain energy for the i^{th} beam element Π_i is given by the following equation:

$$\Pi_i = \frac{1}{2}\int_{V_i} \sigma_i^T \epsilon_{\text{i}}\, \mathrm{d}V_i, \tag{72}$$

where V_i is the volume. Substituting equations (70) and (71) into equation (72), the strain energy can be expressed as follows:

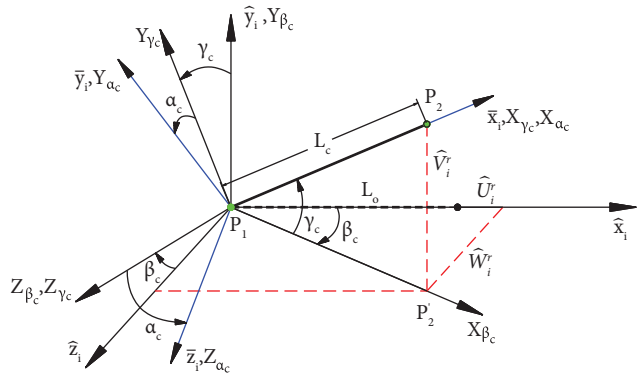

Figure 12: Three successive rotations (β_c, γ_c, α_c) of a three-dimensional beam element.

$$\Pi_i = \frac{1}{2}\int_{V_i}\left(\mathbf{E_i}\,\mathbf{D}_f\,\mathbf{N_i}\,\mathbf{d}_i\right)^T \mathbf{D}_f\,\mathbf{N_i}\,\mathbf{d}_i \quad \mathrm{d}V_i. \tag{73}$$

The element local displacement vector $\mathbf{d}_i$ is independent of the volume V_i. Subsequently, equation (73) can be simplified to the following form:

$$\Pi_i = \frac{1}{2}\,\mathbf{d}_\mathbf{i}^T\mathbf{k}_i\mathbf{d}_i, \tag{74}$$

where $\mathbf{k}_i$ is the symmetric element stiffness matrix in the corotational local coordinate system, which can be defined as follows:

$$\mathbf{k}_i = \int_{V_i}\mathbf{B}^T\,\mathbf{E}_i\,\mathbf{B}\,\mathrm{d}V_\mathbf{i}, \tag{75}$$

and $\mathbf{B}$ is defined as follows:

$$\mathbf{B} = \mathbf{D}_f\,\mathbf{N}_i. \tag{76}$$

Equation (74) can be written as follows:

$$\Pi_i = \frac{1}{2}\,\mathbf{d}_i^{\mathrm{T}}\,\mathbf{k}_i\,\mathbf{d}_i = \frac{1}{2}\left(\mathbf{T}_r\,\mathbf{D}_i\right)^T\mathbf{k}_i\left(\mathbf{T}_r\,\mathbf{D}_i\right) = \mathbf{D}_i^T\,\mathbf{K}_i\,\mathbf{D}_i,$$
$$\mathbf{K}_i = \mathbf{T}_\mathrm{r}^{\mathrm{T}}\,\mathbf{k}_i\,\mathbf{T}_r, \tag{77}$$

where $\mathbf{K}_i$ is the symmetric element stiffness matrix in the fixed global coordinate system.

For the beam element used in this research work, the element stiffness matrix in the local coordinate system $\mathbf{k}_i$ can be expressed as follows:

$$\mathbf{k}_i = \mathbf{k}_1 + \mathbf{k}_2, \tag{78}$$

where $\mathbf{k}_1$ is the axial and bending stiffness matrix and $\mathbf{k}_2$ is the geometric stiffness matrix for the i^{th} beam element. Stiffness matrices are attached in Appendix A.2 and A.3.

5. The Kinetic Energy and the Mass Matrix

The kinetic energy for the i^{th} beam element KE_i is given by the following equation:

$$\mathrm{KE}_i = \frac{1}{2}\int_{V_i}\rho\,\dot{\mathbf{R}}_i^{\mathrm{T}}\,\dot{\mathbf{R}}_i\,\mathrm{d}\,V_i, \tag{79}$$

where $\dot{()}$ is the differentiation with respect to time t, ρ is the density of the i^{th} beam element, and $\dot{\mathbf{R}}_i$ is the velocity of a general point in the i^{th} beam element with respect to the global coordinate system. The velocity of a general point in the i^{th} beam element with respect to the corotational local coordinate system $\dot{\mathbf{r}}_i$ can be expressed as follows:

$$\dot{\mathbf{r}}_i = \mathbf{T}_r\,\dot{\mathbf{R}}_i, \tag{80}$$

where $\dot{\mathbf{r}}_i$ can be written in the following form:

$$\dot{\mathbf{r}}_i = \mathbf{N}_i\,\dot{\mathbf{d}}_i, \tag{81}$$

where $\dot{\mathbf{d}}_i$ is the nodal velocity vector of the i^{th} beam element with respect to the local coordinate system. The vector $\dot{\mathbf{d}}_i$ can be expressed as follows:

$$\dot{\mathbf{d}}_i = \mathbf{T}_r\,\dot{\mathbf{D}}_i, \tag{82}$$

where $\dot{\mathbf{D}}_i$ is the nodal velocity vector of the i^{th} beam element in the global coordinate system. Combining equations (79) and (80), the kinetic energy can be written as follows:

$$\mathrm{KE}_i = \frac{1}{2}\int_{V_i}\rho\left(\mathbf{N}_i\,\mathbf{T}_r\,\dot{\mathbf{D}}_i\right)^T\left(\mathbf{N}_i\,\mathbf{T}_r\,\dot{\mathbf{D}}_i\right)\mathrm{d}V_i. \tag{83}$$

The velocity vector $\dot{\mathbf{D}}_i$ and the transformation matrix $\mathbf{T}_r$ are independent of the volume V_i. Subsequently, equation (83) can be simplified to the following form:

$$\mathrm{KE}_i = \frac{1}{2}\,\dot{\mathbf{D}}_i^T\,\mathbf{T}_r^T \quad \mathbf{m}_i\,\mathbf{T}_r\,\dot{\mathbf{D}}_i, \tag{84}$$

where $\mathbf{m}_i$ is the symmetric element mass matrix in the local corotational coordinate system defined as follows:

$$\mathbf{m}_i = \frac{1}{2}\int_{V_i}\rho\,\mathbf{N}_i^T\,\mathbf{N}_i\,\mathrm{d}\,V_i. \tag{85}$$

Equation (84) can be written in the following form:

$$\mathrm{KE}_i = \frac{1}{2}\,\dot{\mathbf{D}}_i^{\mathrm{T}} \quad \mathbf{M}_i \quad \dot{\mathbf{D}}_i, \tag{86}$$

where $\mathbf{M}_i$ is the symmetric element mass matrix in the fixed global coordinate system defined as follows:

$$\mathbf{M}_i = \mathbf{T}_r^T\,\mathbf{m}_i\,\mathbf{T}_r. \tag{87}$$

For the beam element used in this research work, the element mass matrix in the local coordinate system $\mathbf{m}_i$ can expressed as follows:

$$\mathbf{m}_i = \mathbf{m}_1 + \mathbf{m}_2, \tag{88}$$

where m_1 is the ith beam element mass matrix for the translational inertia and m_2 is the mass matrix of the i^{th} beam element for the rotational inertia. The mass matrices are attached in Appendices A.4 and A.5.

It is worth mentioning that the rotation is noncommutative. However, in our analysis, we used the three-coordinate system that separates the large rigid-body motion from the internal deformation. We restrict our analysis to the small strain theory, as we mention in subsection (2.1), and the internal rotational displacements within each element in each time step are always small. Therefore, the usual vector addition rules can be applied to these rotational displacements. Hence, the obtained stiffness and mass matrices are symmetric.

6. The Equation of Motion

Lagrange's equation reported by [36, 37] is used to derive the equation of motion in this section. It can be written for the i^{th} beam element as follows:

$$\frac{d}{dt}\left(\frac{\partial \text{KE}_i}{\partial \dot{\mathbf{D}}_i}\right)^T - \left(\frac{\partial \text{KE}_i}{\partial \mathbf{D}_i}\right)^T + \left(\frac{\partial \Pi_i}{\partial \mathbf{D}_i}\right)^T = \left(\frac{\partial \text{WD}_i}{\partial \mathbf{D}_i}\right)^T, \tag{89}$$

where KE_i is the kinetic energy, Π_i is the strain energy, WD_i is the work done by the external forces, $\dot{\mathbf{D}}_i$ is the nodal velocity vector in the global coordinate system, and $\mathbf{D}_i$ is the nodal displacement vector in the global coordinate system. The work done by the external forces on the i^{th} beam element is given by the following equation:

$$\text{WD}_i = \mathbf{D}_i^T \mathbf{F}_i^P, \tag{90}$$

where F_i^P is the vector of the external applied forces on the i^{th} beam element in the fixed global coordinate system.

Using equation (86), one can write the first two terms in the left-hand side of the previous relation as follows:

$$\frac{d}{dt}\left(\frac{\partial \text{KE}_i}{\partial \dot{\mathbf{D}}_i}\right)^T - \left(\frac{\partial \text{KE}_i}{\partial \mathbf{D}_i}\right)^T = \mathbf{M}_i \ddot{\mathbf{D}}_i. \tag{91}$$

Using equation (77), the third term in the left-hand side of equation (89) can be written as follows:

$$\left(\frac{\partial \Pi_i}{\partial \mathbf{D}_i}\right)^T = \mathbf{K}_i \mathbf{D}_i. \tag{92}$$

Also, one can write

$$\left(\frac{\partial \text{WD}_i}{\partial \mathbf{D}_i}\right)^T = \mathbf{F}_i^P. \tag{93}$$

Substituting equations (91)–(93) in equation (89), one obtains

$$\mathbf{M}_i \ddot{\mathbf{D}}_i + \mathbf{K}_i \mathbf{D}_i = \mathbf{F}_i^P. \tag{94}$$

One can write

$$\mathbf{F}_i^e = \mathbf{K}_i \mathbf{D}_i = \mathbf{T}_r^T \mathbf{f}_i^e, \tag{95}$$

where $\mathbf{F}_i^e$ is the internal elastic force vector in the fixed global and $\mathbf{f}_i^e$ is the internal elastic force vector in the local coordinate systems, which is given by

$$\mathbf{f}_i^e = \mathbf{k}_i \mathbf{d}_i. \tag{96}$$

Substituting equation (95) in equation (94) gives

$$\mathbf{F}_i^e + \mathbf{M}_i \ddot{\mathbf{D}}_i - \mathbf{F}_i^P = 0. \tag{97}$$

Equation (97) is the equation of motion of the i^{th} beam element. Assembling the element force vectors, acceleration vectors, and mass matrices leads to the equation of motion of the overall structure, which takes the following form:

$$\mathbf{F}^e + \mathbf{M}\ddot{\mathbf{D}} - \mathbf{F}^P = \mathbf{0}, \tag{98}$$

where $\mathbf{F}^P$ is the vector of the external applied forces of the entire structure and $\mathbf{F}^e$ is the internal elastic force vector of the entire structure. Both $\mathbf{F}^P$ and $\mathbf{F}^e$ are defined in the fixed global coordinate system. $\mathbf{M}$ is the mass matrix in the global coordinate system of the entire structure, and $\ddot{\mathbf{D}}$ is the acceleration vector in the global coordinate system of the entire structure. Rayleigh damping is used in equation (98) to read

$$\mathbf{F}^e + \mathbf{C}\dot{\mathbf{D}} + \mathbf{M}\ddot{\mathbf{D}} - \mathbf{F}^P = \mathbf{0}, \tag{99}$$

where $\mathbf{C}$ is the damping matrix in the global coordinate system of the entire structure and $\dot{\mathbf{D}}$ is the velocity vector in the global coordinate system of the entire structure. The damping matrix $\mathbf{C}$ is defined in terms of the stiffness matrix and the mass matrix as follows:

$$\mathbf{C} = \mu \mathbf{M} + \eta \mathbf{K}, \tag{100}$$

where μ and η are the damping coefficient which can be determined from the vibration modes of the system. $\mathbf{K}$ is the assembled stiffness matrix in the global coordinate system of the entire structure.

7. Numerical Algorithms

The equation of motion is solved using an incremental iterative procedure. This procedure is based on the full Newton–Raphson and the Newmark direct integration implicit method [13, 38]. Equation (99) can be rewritten as follows:

$$\boldsymbol{\psi} = \mathbf{F}^e + \mathbf{C}\dot{\mathbf{D}} + \mathbf{M}\ddot{\mathbf{D}} - \mathbf{F}^P = \mathbf{0}, \tag{101}$$

where $\boldsymbol{\psi}$ is the out of balance force. The iteration equilibrium convergence criterion is given by the following equation:

$$\|\boldsymbol{\psi}\| \le e_r \|\boldsymbol{\psi}_{\mathbf{f}}\|, \tag{102}$$

where $\boldsymbol{\psi}_{\mathbf{f}}$ is the reference out of balance force, which is assumed to be the out of balance force in the first iteration, and e_r is the error tolerance.

It is worth mentioning that it is well known that element matrices are used only in the iterative process for the incremental solution, and they do not have to be exact. They are

required to allow the solution to converge and satisfy the specified tolerance during the solution iterations. That is why many authors have used tangent, secant, or even initial stiffness matrices in their nonlinear FE formulations. Using exact matrices typically costs more time because of the storage of nonsymmetric matrices compared with the storage of only the triangular part in the symmetric matrices. Therefore, we are confident that the restriction we made in subsection (2.1), which produced symmetric stiffness matrices, allows the whole solution to go faster without affecting the overall accuracy of the results. Through the solution of various numerical examples in the next section, we have assessed the effectiveness and the accuracy of this method.

At the beginning of the solution, it is assumed that the displacement, velocity, and acceleration vectors are null. The values of the vectors $\mathbf{D}$, $\dot{\mathbf{D}}$, and $\ddot{\mathbf{D}}$, at a known equilibrium configuration and time $t = t_N$, are $\mathbf{D}_N$, $\dot{\mathbf{D}}_N$, and $\ddot{\mathbf{D}}_N$, respectively. Likewise, the values of $\mathbf{D}$, $\dot{\mathbf{D}}$, and $\ddot{\mathbf{D}}$, at time $t = t_N + \Delta t$, are $\mathbf{D}_{N+1}$, $\dot{\mathbf{D}}_{N+1}$, and $\ddot{\mathbf{D}}_{N+1}$, where Δt is the time step. Using the geometric data, one can search for vertical member, which is handled differently, as stated in Section 3. The numerical solution procedure is described in the following steps at the beginning of each time step:

(i) Compute $\mathbf{k}_i$, $\mathbf{m}_i$, and $\mathbf{f}_i^e$ for each element using equations (78), (88) and (96), respectively.

(ii) In the first iteration, calculate the matrices $\mathbf{r}_o$ and $\mathbf{T}_o$ using equations (25) and (41). In all other iterations, calculate $\mathbf{r}_c$ and $\mathbf{T}_c$ using equations (27) and (66).

(iii) Determine the transformation matrix $\mathbf{T}_r$ for each member using equation (30).

(iv) Obtain $\mathbf{K}_i$, $\mathbf{M}_i$, and $\mathbf{F}_i^e$ according to equations (77), (87), and (95).

(v) Get $\mathbf{K}$, $\mathbf{M}$, and $\mathbf{F}^e$ for the entire structure, by assembling the stiffness matrices, the mass matrices, and the internal elastic force vectors for all elements of the analysed structure.

(vi) Calculate the out of balance force $\boldsymbol{\psi}$ from equation (101).

(vii) If the convergence condition in equation (102) is satisfied, stop the iteration and go to step ix. Otherwise, start the following iteration:

(a) Using the Newton–Raphson method, a displacement corrector vector $\mathbf{R}$ is calculated as follows:

$$\mathbf{R} = -\overline{\mathbf{K}}^{-1}\boldsymbol{\psi}, \tag{103}$$

where $\overline{\mathbf{K}}$ is the effective matrix that can be defined as follows:

$$\overline{\mathbf{K}} = \frac{1}{\tau\,\Delta t^2}\mathbf{M} + \frac{\exists}{\tau\Delta t}\mathbf{C} + \mathbf{K}, \tag{104}$$

where τ and $\exists$ are the Newmark parameters [38].

(b) Update the incremental displacement vector as follows:

$$\Delta\mathbf{D} = \Delta\mathbf{D}_0 + \mathbf{R}, \tag{105}$$

where $\Delta\mathbf{D}_0$ is the incremental displacement vector in the previous iteration, which is considered to be zero in the first iteration.

(c) Extract vector $\Delta\mathbf{D_i}$ for each element from vector $\Delta\mathbf{D}$. Consequently, one can update the vectors $\mathbf{D_i}$ and $\mathbf{X}_i$ using equations (3) and (7).

(d) Using $\mathbf{D_i}$ and $\mathbf{r}_o$, the relative displacements are calculated, as in equations (49)–(51).

(e) From the coordinate vector $\mathbf{X}_i$, the model can check for each element position to apply either the regular rotations matrices in equations (42), (57), and (65) or the vertical member rotations matrices in equations (45), (58), and (65). Then, $\mathbf{T}_c$ and $\mathbf{T}_r$ are updated for each element.

(f) Using the relative displacements, the rigid-body rotations can be obtained as follows:

$$\mu_Y = \tan^{-1}\left(\frac{\hat{W}_i^r}{\sqrt{\left(L_o + \hat{U}_i^r\right)^2}}\right),$$
$$\mu_Z = \tan^{-1}\left(\frac{\hat{V}_i^r}{\sqrt{\left(L_o + \hat{U}_i^r\right)^2 + \left(\hat{W}_i^r\right)^2}}\right). \tag{106}$$

(g) Eliminate the rigid-body rotations from the rotational components θY_n and θZ_n in the vector $\mathbf{D}_i$, for each element, as follows:

$$\theta\grave{Y}_n = \theta Y_n + \mu_Y,$$
$$\theta\grave{Z}_n = \theta Z_n - \mu_z. \tag{107}$$

(h) Transform the pure rotations $\theta X_n.\theta\grave{Y}_n$ and $\theta\grave{Z}_n$, which are relative to the fixed global frame, to determine the corresponding rotational components $\theta x_n.\ \theta y_n$ and θz_n for vector $\mathbf{d}_i$ in the current corotational local frame which are always relative to the element chord, using the procedure detailed in equations (24) and (26).

(i) The axial displacement u_2 in equation (17) is obtained from equation (23).

(j) Using equations (17) and (96), $\mathbf{d}_i$ and $\mathbf{f}_i^e$ can be determined, respectively.

(k) Using the Newmark direct integration method [38], $\dot{\mathbf{D}}_{N+1}$ and $\ddot{\mathbf{D}}_{N+1}$ can be calculated as follows:

$$\ddot{\mathbf{D}}_{N+1} = \frac{\Delta\mathbf{D}}{\tau\,\Delta t^2} - \frac{\dot{\mathbf{D}}_N}{\tau\Delta t} - \left(\frac{1}{2\,\tau} - 1\right)\ddot{\mathbf{D}}_N,$$
$$\dot{\mathbf{D}}_{N+1} = \dot{\mathbf{D}}_N + \Delta t\left((1 - \exists)\ddot{\mathbf{D}}_N + \exists\ddot{\mathbf{D}}_{N+1}\right). \tag{108}$$

(viii) Going to the start of step iv again.

(ix) The displacement vector at time $t = t_N + \Delta t$ can be updated as follows:

$$\mathbf{D}_{N+1} = \mathbf{D}_N + \Delta\mathbf{D}. \quad (109)$$

(x) Start the next time step.

It should be noted that this code includes a detection function in the MATLAB code, which accurately determines the position of each element using the nodal coordinate vector. Thus, it can easily select the appropriate trigonometric rules and the sign of rotations. The detection function specifies the position of the element using the nodal coordinate vector $\mathbf{X}_i$ given in equation (7). When the relative difference between the coordinate in X and Z direction of the element end nodes approaches zero together, the code detects that the angle β_c turns to be zero and the element is in the direction of the Y axis. In this case, the code searches for the alignment of the element based on the sign of $C_Y^{'}$ in equation (59). In addition, when the relative displacement $\hat{V}_i^{r}$ turns out to be zero, the angle γ_c vanishes. Likewise, if the relative displacement $\hat{W}_i^{r}$ turns out to be zero, the angle β_c vanishes; however, the element in general is not vertical. Hence, the program deals with these special cases separately.

This function also controls the angle γ_c when the rotation is outside the interval $[\pi/2, -\pi/2]$. The sign SN in equation (53) specifies the cosine of the angle γ_c to meet the corresponding element position during the motion because the terms $\overline{P_1P_2'}$ and L_c are always positive which cannot reflect the real sign of cosine of γ_c. At the same time, the sine of γ_c is already specified with the sign of $\hat{V}_i$. This function conserves the code to converge efficiently. This numerical algorithm steps are organized in Figure 13.

8. Numerical Examples

8.1. Simple Supported Beam Subjected to a Concentrated Step Load. The first example is a simply supported beam whose geometric properties are $L = 12$ m, $A = 8.06 \text{ X } 10^{-3}\text{m}^2$, and $I_Y = I_Z = 1.858 \text{ X } 10^{-4}\text{m}^4$ and material properties are $E = 210$ GPa, $G = 80.775$ GPa, and $\rho = 7850$ kg/m^3, as shown in Figure 14. The beam is subjected to a vertical concentrated load, at point C, which increases linearly to reach the value of 10 KN at 0.15 second before being steady, as can be seen in Figure 15. Six beam elements are used in the analysis, and time step $\Delta t = 5 \text{ X } 10^{-4}$ s and the error tolerance e_r is chosen to be 10^{-4}. Liu [6] solved this problem using a corotational formulation based on Euler's theorem. He compared his results with the theoretical results [6]. The present results are compared with the results in [6], as shown in Figure 16. This comparison reveals that the present results remarkably agreed with the theoretical results in [6].

8.2. Clamped-Clamped Beam Subjected to a Concentrated Vertical Load at the Midspan. In this part, a clamped-clamped beam is analysed. The geometric data of the beam are shown in Figure 17. The beams modulus of elasticity equals 30,000 ksi, density is 0.098 lb/in^3, and Poisson's ratio is considered to be zero. This beam is subjected to a dynamic concentrated step load. This load is assumed to be applied suddenly to the midspan, as can be shown in Figure 18. This problem is solved by Mondkar and Powell [39] using various time steps. A secant stiffness concept is utilized to solve this problem by Chan [40]. The present results are obtained using ten element and error tolerance $e_r = 10^{-2}$. The present results are compared with the results of [39] and the linear analysis results, using the same time step $\Delta t = 50\mu$s. The dynamic load is applied over a period of 5000 μs (0.005 s). As can be shown in Figure 19, the present results are significant in agreement with the results in [39]. Figure 19 also clarifies the considerable differences between linear and the nonlinear results. Another comparison is made between the present results, the results of Chan [40], and the results of Mondkar and Powell [39]. In this comparison, the time step is $\Delta t = 100\mu$s and the time duration is 10000 μs (0.01 s). These results are compared with the so-called exact solution in [39], which is obtained by using a shorter time step of $\Delta t = 25\,\mu$s. Figure 20 reveals that the present results are closer to the so-called exact solution than the other results.

8.3. Damped Cantilever Beam Subjected to a Ramp-Ramp Load at the Free End. In this example, a cantilever beam subjected to a ramp-ramp dynamic load is presented, as shown in Figures 21 and 22. The geometric data of the beam are $L = 120$ in (0.508 m), $A = 21.9$ in^2 (0.014 m^2), and $I_Y = I_Z = 100$ in^4 (4.16×10^{-5} m^4). The material density ρ is 4.567×10^{-3} lb.s^2/in^4 (4.8808×10^4 kg/m^3), the modulus of elasticity $E = 30 \times 10^6$ psi (207 GPa), and Poisson's ratio $\nu = 0.3$. In this example, a viscous damping coefficient equal to 10 lb/in/s (1.7513×10^3 N/m/s) is applied for each translational degree of freedom. This problem is classified as a large rotation and large displacement problem [6]. Liu [6] solved this problem using a lumped mass matrix using eight elements. However, he did not clarify the time step used in the analysis. Behdinan et al. [41] also analysed this problem using two different formulations, the consistent corotational formulation and the updated Lagrangian formulation. They used a different time step in each formulation. However, they did not specify clearly the time step used in each formulation. The present results are obtained using eight elements, with the error tolerance $e_r = 10^{-2}$ and time step $\Delta t = 1 \text{ x } 10^{-3}$. These results are compared with the results in [6, 41]. This comparison clearly shows that the results are well consistent, as shown in Figure 23.

8.4. Cantilever Beam Subjected to a Sinusoidal-Concentrated End Load and a Concentrated End Moment. A cantilever beam of length $L = 10$ m with uniform cross section, as can be seen in Figure 24, is solved in this section. The beam is subjected to a vertical concentrated sinusoidal out of plane dynamic force $F_Z(t)$ and a bending moment $M_Z(t)$ at the free end, as shown in Figure 25. The circular frequency of the force is $\omega = 50$ rad/s, Young's modulus E is 210 GPa, material's density is $\rho = 7{,}850$ kg/m^3, and Poisson's ratio is $\nu = 0.3$. The dimensions of the cross section are $e = 0.25$ m and $a = 0.3$ m. Ten beam elements are used in the analysis, time step is $\Delta t = 5 \text{ x } 10^{-4}$ s, and the error tolerance is $e_r = 10^{-2}$. Le et al. [26] solved this problem using two different beam elements (cubic and linear) based on spatial spin variables and spatial rotational vector as a parametrization method for finite rotations. They

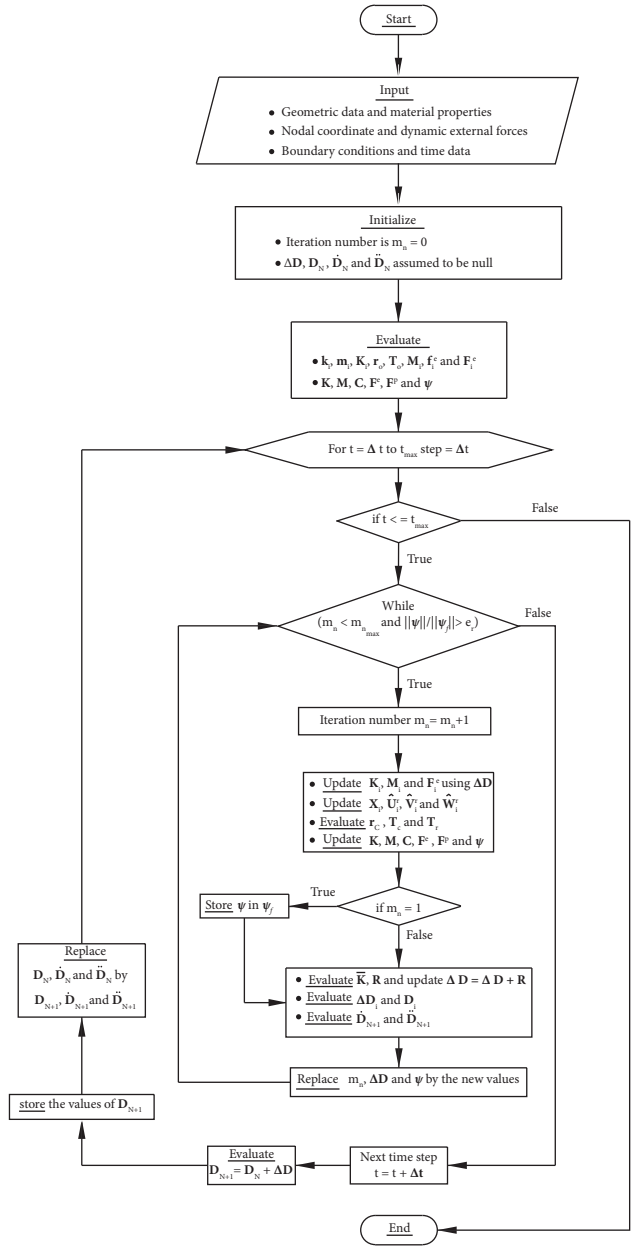

Figure 13: The solution strategy.

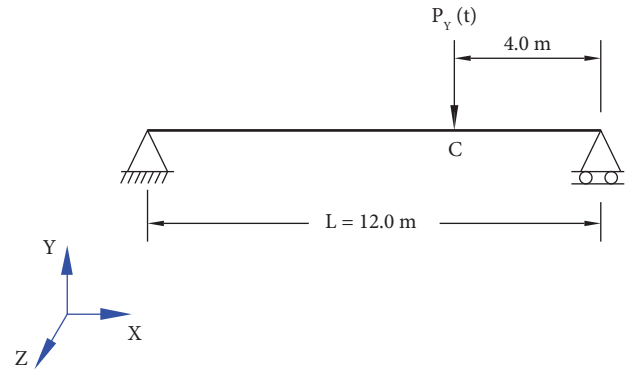

Figure 14: Geometrical data for the simply supported beam.

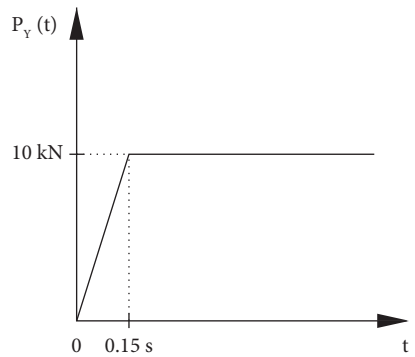

Figure 15: The dynamic load history of the simply supported beam.

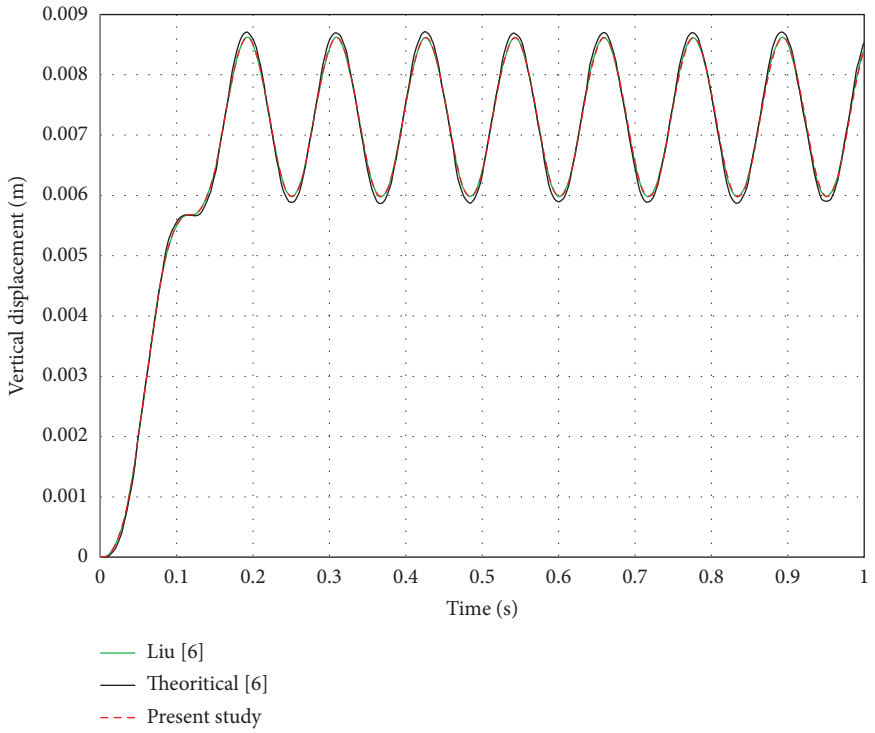

Figure 16: Time-vertical displacement at the point C curve for the simply supported beam.

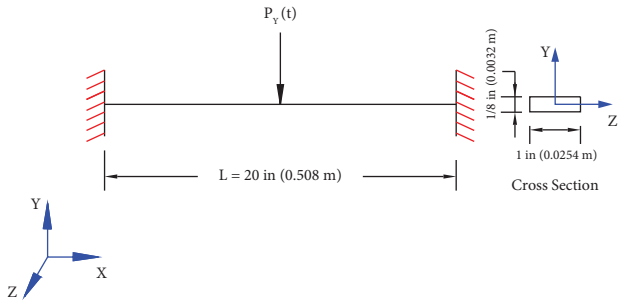

Figure 17: Geometrical data of the clamped-clamped beam.

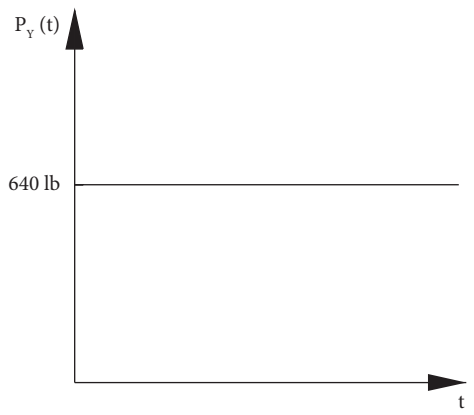

Figure 18: The dynamic load history of the clamped-clamped beam.

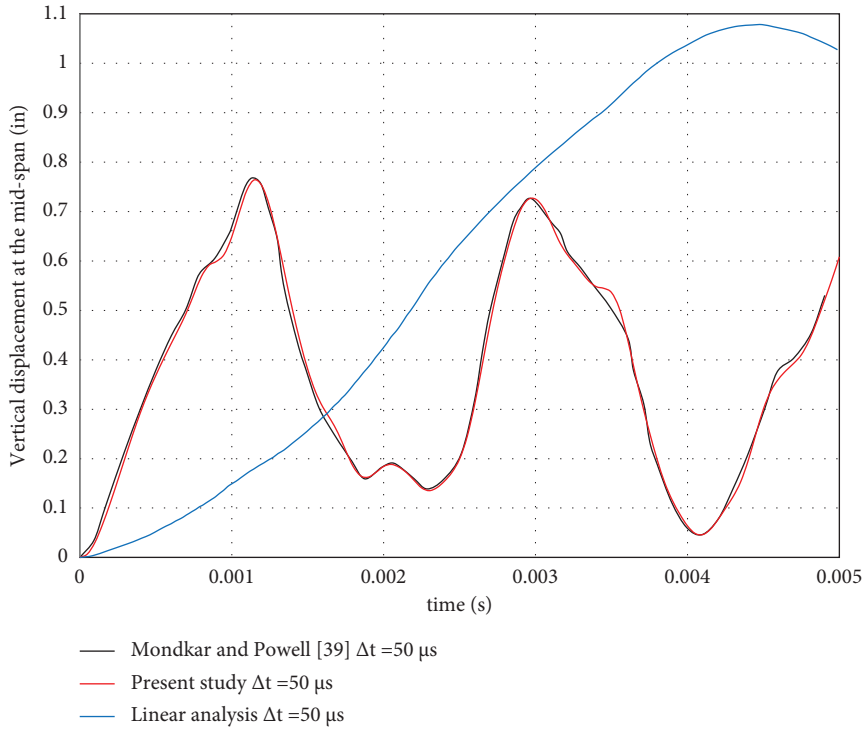

Figure 19: Comparison of dynamic responses of the clamped-clamped beam with $\Delta t = 50\,\mu s$.

obtained a reference solution with 20 beam elements. They also compared their results with the results of Simo and Vu-Quoc [42]. The results of the proposed formulation are closer to the so-called reference solution than the results of other formulations given in [26], as shown in Figures 26–28.

8.5. A Right Angle Cantilever Beam Subjected to a Sinusoidal-Concentrated End Load. A right-angle cantilever beam is solved, as shown in Figure 29. This problem is classified as a three-dimensional large deformation problem [6]. The geometric properties of the beam are $A = 21.9\text{in}^2$ (0.014m^2) and $I_Y = I_Z = 100\text{in}^4$ $(4.16\,\text{X}\,10^{-5}\text{m}^4)$ and material properties are $E = 30\,\text{X}\,10^6$ psi (207 GPa) and mass density $\rho = 4.567\,\text{X}\,10^{-3}\,\text{lb}.s^2/\text{in}^3$ $(126.4\,\text{kg}.s^2/\text{m}^3)$. The beam is subjected to a concentrated vertical sinusoidal dynamic force $F_Y(t) = 500000 \sin(50t)\text{lb}$ $(2224 \sin(50t)\,\text{kN})$. Liu [6] solved this problem using eight elements with lumped mass. He compared his results with the results of ANSYS program using the same number of elements. Eight beam elements are used in the proposed analysis, time step is $\Delta t = 3\,\text{x}\,10^{-4}$ s, and the error tolerance is $e_r = 10^{-2}$. The present results are compared with the results in [6], as can be seen in Figure 30. This comparison shows that the present results are in agreement with the results in [6].

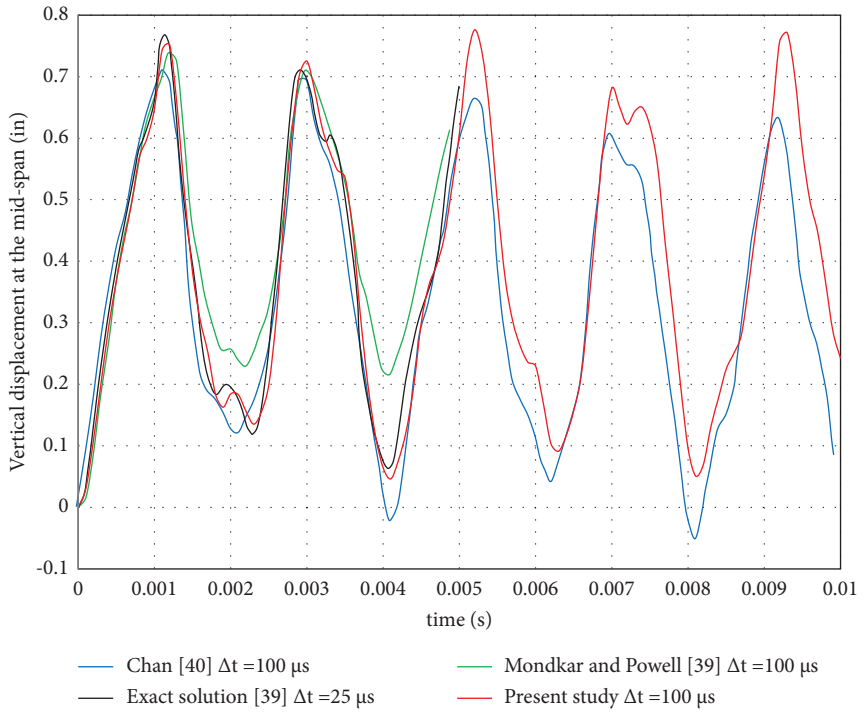

Figure 20: Comparison of dynamic responses of the clamped-clamped beam with $\Delta t = 100\,\mu s$.

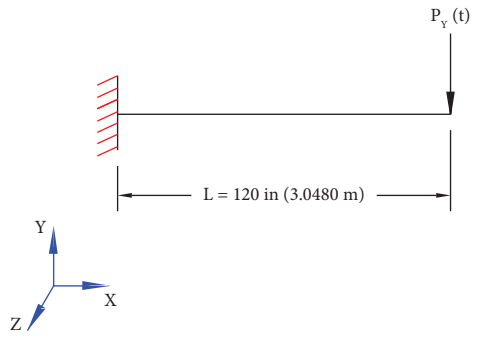

Figure 21: Geometrical data of the cantilever beam.

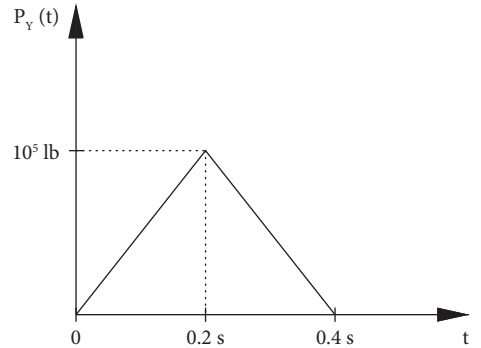

Figure 22: The dynamic load history of the cantilever beam.

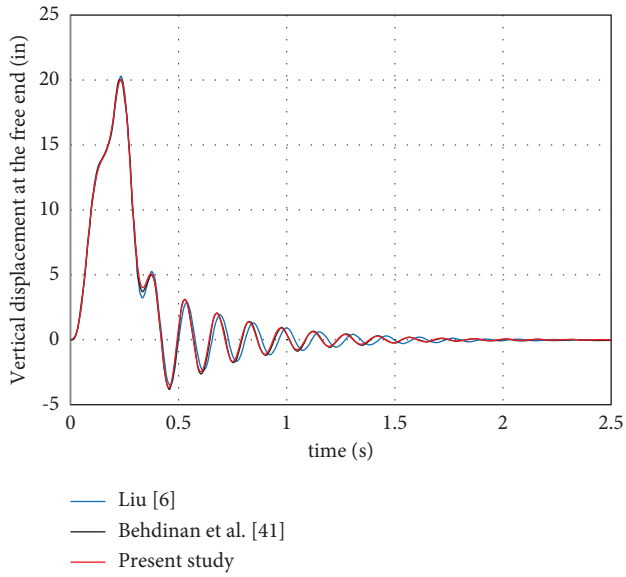

Figure 23: Time-tip displacement curve for the cantilever beam.

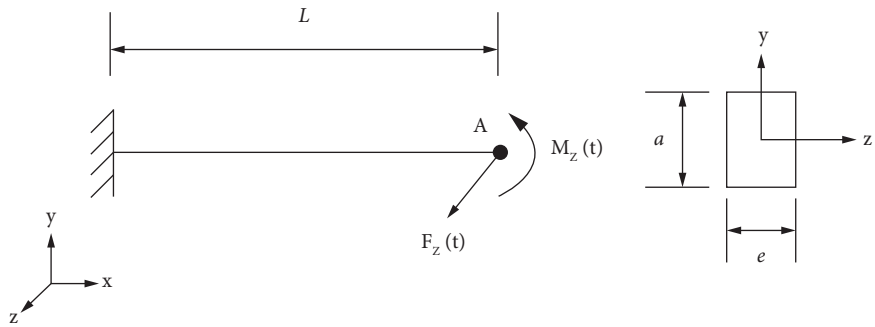

Figure 24: Geometrical data of the cantilever beam.

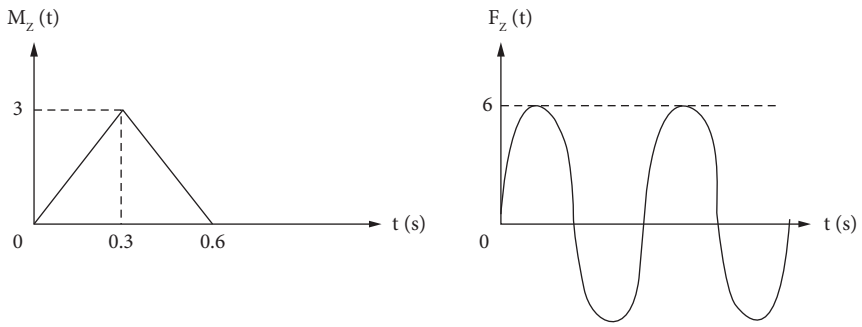

Figure 25: The cantilever beam load history.

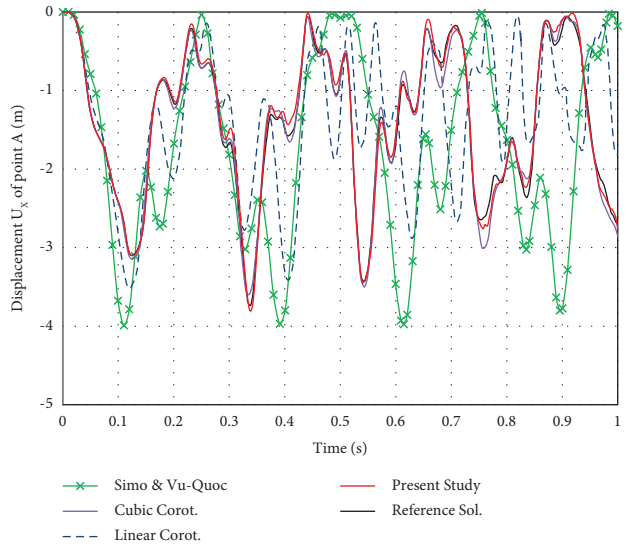

FIGURE 26: Time-displacement U_X of the point A curve for the cantilever beam.

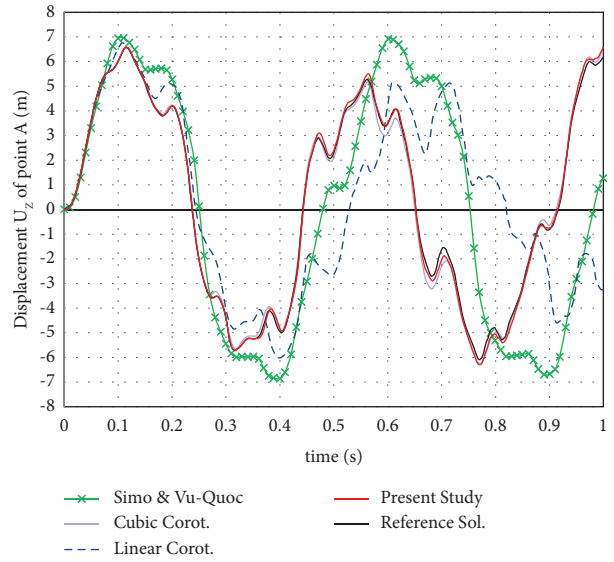

FIGURE 27: Time-displacement U_Z of the point A curve for the cantilever beam.

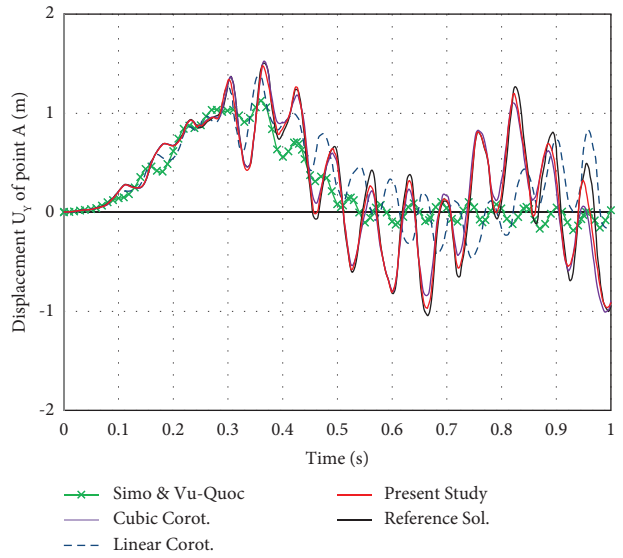

FIGURE 28: Time-displacement U_Y of the point A curve for the cantilever beam.

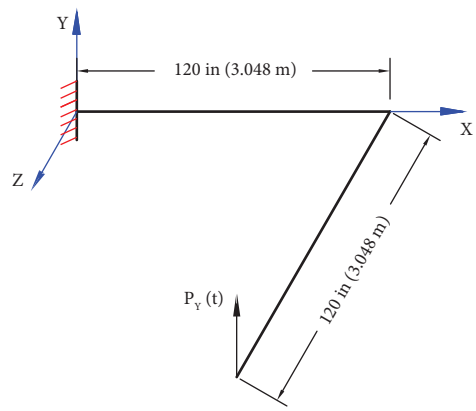

Figure 29: Geometrical data of the right-angle frame.

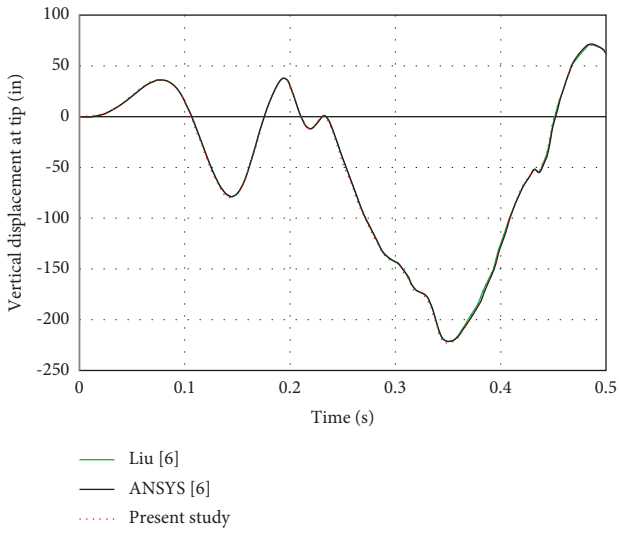

Figure 30: The dynamic response of the right-angle frame.

9. Conclusion

A modified corotational finite element formulation for geometrically nonlinear dynamic analysis of spatial beams and frames has been presented in this paper. The following points are the main outcomes of this study:

(i) Owing to the nature of the used corotational frame, which continuously updates and translates with each element, the used formulation condenses the computed local displacement vector compared to other formulations. In addition, it can smoothly separate the rigid-body rotations from the deformational rotations.

(ii) Since the deformation is always small with respect to the corotational frame, the small strain theory has been applied. Accordingly, the stiffness and mass matrices are symmetric which significantly reduces the required storage memory and consequently reduces the computational time and improves the convergence rate.

(iii) A two-stage procedure is proposed to transform vectors and matrices from the fixed global frame to the moving corotational frame. This procedure depends essentially on Tait–Bryan angles, which are computed successively. Trigonometric rules for all rotation angles with their different cases have been defined in terms of kinematics parameters. Accordingly, the proposed method deals with the problems of the vertical members and the rotation angles greater than $\pi/2$. This contribution has been used for handling some of the reported cases which are classified as singularity problems.

(iv) For the numerical solution, an incremental iterative method based on the full Newton–Raphson method and the Newmark direct integration implicit method has been used to solve the equations of motion. A MATLAB code has been written for this purpose. This code includes detection functions, which successfully control the sign of rotations during the analysis. Therefore, no convergence problems have been detected throughout the study.

(v) Each iteration, the element coordinate, stiffness, and mass matrices are updated regularly. Though this updating requires time in each iteration, it significantly decreases the overall time of the analysis.

(vi) The results have been compared with the published results to show the effectiveness and accuracy of the proposed formulation and the numerical algorithm. Though these problems have been solved using an adequate number of elements, accurate results have been obtained compared with the published results.

(vii) The proposed formulation provides a rapid convergence rate and does not need special parametrization for finite rotations. However, it requires

the adjustment of the time step and the element size in order to adjust the relative chordal rotations during each time step.

Appendix

A.1. The Shape Function Matrix

$$\mathbf{N}_i = \begin{bmatrix} N_1 & 0 & 0 & 0 & 0 & 0 & N_4 & 0 & 0 & 0 & 0 & 0 \\ 0 & N_2 & 0 & 0 & 0 & N_3 & 0 & N_5 & 0 & 0 & 0 & N_6 \\ 0 & 0 & N_2 & 0 & -N_3 & 0 & 0 & 0 & N_5 & 0 & -N_6 & 0 \\ 0 & 0 & 0 & N_1 & 0 & 0 & 0 & 0 & 0 & N_4 & 0 & 0 \\ 0 & 0 & N_2^{'} & 0 & -N_3^{'} & 0 & 0 & 0 & N_5^{'} & 0 & -N_6^{'} & 0 \\ 0 & N_2^{'} & 0 & 0 & 0 & N_3^{'} & 0 & N_5^{'} & 0 & 0 & 0 & N_6^{'} \end{bmatrix}, \tag{A.1}$$

where $(\,)^{'}$ is the first derivatives with respect to $\overline{x}_i$.

A.2. The Axial and Bending Stiffness Matrix

$$\mathbf{k_1} = \begin{bmatrix} \frac{Ea_i}{L_o} & 0 & 0 & 0 & 0 & 0 & -\frac{Ea_i}{L_o} & 0 & 0 & 0 & 0 & 0 \\ 0 & \frac{12EI_{zi}}{L_o^3} & 0 & 0 & 0 & \frac{6EI_{zi}}{L_o^2} & 0 & -\frac{12EI_{zi}}{L_o^3} & 0 & 0 & 0 & \frac{6EI_{zi}}{L_o^2} \\ 0 & 0 & \frac{12EI_{yi}}{L_o^3} & 0 & -\frac{6EI_{yi}}{L_o^2} & 0 & 0 & 0 & -\frac{12EI_{yi}}{L_o^3} & 0 & -\frac{6EI_{yi}}{L_o^2} & 0 \\ 0 & 0 & 0 & \frac{GJ_i}{L_o} & 0 & 0 & 0 & 0 & 0 & -\frac{GJ_i}{L_o} & 0 & 0 \\ 0 & 0 & -\frac{6EI_{yi}}{L_o^2} & 0 & \frac{4EI_{yi}}{L_o} & 0 & 0 & 0 & \frac{6EI_{yi}}{L_o^2} & 0 & \frac{2EI_{yi}}{L_o} & 0 \\ 0 & \frac{6EI_{zi}}{L_o^2} & 0 & 0 & 0 & \frac{4EI_{zi}}{L_o} & 0 & -\frac{6EI_{zi}}{L_o^2} & 0 & 0 & 0 & \frac{2EI_{zi}}{L_o} \\ -\frac{Ea_i}{L_o} & 0 & 0 & 0 & 0 & 0 & \frac{Ea_i}{L_o} & 0 & 0 & 0 & 0 & 0 \\ 0 & -\frac{12EI_{zi}}{L_o^3} & 0 & 0 & 0 & -\frac{6EI_{zi}}{L_o^2} & 0 & \frac{12EI_{zi}}{L_o^3} & 0 & 0 & 0 & -\frac{6EI_{zi}}{L_o^2} \\ 0 & 0 & -\frac{12EI_{yi}}{L_o^3} & 0 & \frac{6EI_{yi}}{L_o^2} & 0 & 0 & 0 & \frac{12EI_{yi}}{L_o^3} & 0 & \frac{6EI_{yi}}{L_o^2} & 0 \\ 0 & 0 & 0 & -\frac{GJ_i}{L_o} & 0 & 0 & 0 & 0 & 0 & \frac{GJ_i}{L_o} & 0 & 0 \\ 0 & 0 & -\frac{6EI_{yi}}{L_o^2} & 0 & \frac{2EI_{yi}}{L_o} & 0 & 0 & 0 & \frac{6EI_{yi}}{L_o^2} & 0 & \frac{4EI_{yi}}{L_o} & 0 \\ 0 & \frac{6EI_{zi}}{L_o^2} & 0 & 0 & 0 & \frac{2EI_{zi}}{L_o} & 0 & -\frac{6EI_{zi}}{L_o^2} & 0 & 0 & 0 & \frac{4EI_{zi}}{L_o} \end{bmatrix}, \tag{A.2}$$

where E is the modulus of elasticity, G is the modulus of rigidity, a_i is the cross-sectional area, I_{y_i} and I_{Zi} are the moment of inertia about $\hat{y}_i$ and $\hat{z}_i$ axes, and J_i is the polar moment of inertia.

A.3. The Geometric Stiffness Matrix

$$\mathbf{k_2} = \frac{\mathrm{fx_2}}{\mathrm{L_o}} \begin{bmatrix} 0 & 0 & 0 & 0 & 0 & 0 & 0 & 0 & 0 & 0 & 0 & 0 \\ 0 & \frac{6}{5} & 0 & 0 & 0 & \frac{1}{10}L_o & 0 & -\frac{6}{5} & 0 & 0 & 0 & \frac{1}{10}L_o \\ 0 & 0 & \frac{6}{5} & 0 & -\frac{1}{10}L_o & 0 & 0 & 0 & -\frac{6}{5} & 0 & -\frac{1}{10}\mathrm{L_o} & 0 \\ 0 & 0 & 0 & 0 & 0 & 0 & 0 & 0 & 0 & 0 & 0 & 0 \\ 0 & 0 & -\frac{1}{10}L_o & 0 & -\frac{2}{15}L_o^2 & 0 & 0 & 0 & \frac{1}{10}L_o & 0 & -\frac{1}{30}L_o^2 & 0 \\ 0 & \frac{1}{10}L_o & 0 & 0 & 0 & \frac{2}{15}L_o^2 & 0 & -\frac{1}{10}L_o & 0 & 0 & 0 & -\frac{1}{30}L_o^2 \\ 0 & 0 & 0 & 0 & 0 & 0 & 0 & 0 & 0 & 0 & 0 & 0 \\ 0 & -\frac{6}{5} & 0 & 0 & 0 & -\frac{1}{10}L_o & 0 & \frac{6}{5} & 0 & 0 & 0 & -\frac{1}{10}L_o \\ 0 & 0 & -\frac{6}{5} & 0 & \frac{1}{10}L_o & 0 & 0 & 0 & \frac{6}{5} & 0 & \frac{1}{10}L_o & 0 \\ 0 & 0 & 0 & 0 & 0 & 0 & 0 & 0 & 0 & 0 & 0 & 0 \\ 0 & 0 & -\frac{1}{10}L_o & 0 & -\frac{1}{30}L_o^2 & 0 & 0 & 0 & \frac{1}{10}L_o & 0 & \frac{2}{15}L_o^2 & 0 \\ 0 & \frac{1}{10}L_o & 0 & 0 & 0 & -\frac{1}{30}L_o^2 & 0 & -\frac{1}{10}L_o & 0 & 0 & 0 & \frac{2}{15}L_o^2 \end{bmatrix}, \tag{A.3}$$

where fx_2 is the axial force of the second node in $\overline{x}_i$ direction, which is presented in equation (11).

A.4. The Mass Matrix for the Translational Inertia

$$\mathbf{m_1} = \begin{bmatrix} \frac{\rho a_i L_o}{3} & 0 & 0 & 0 & 0 & 0 & \frac{\rho a_i L_o}{6} & 0 & 0 & 0 & 0 & 0 \\ 0 & \frac{13\rho a_i L_o}{35} & 0 & 0 & 0 & \frac{11\rho a_i L_o^2}{210} & 0 & \frac{9\rho a_i L_o}{70} & 0 & 0 & 0 & -\frac{13\rho a_i L_o^2}{420} \\ 0 & 0 & \frac{13\rho a_i L_o}{35} & 0 & -\frac{11\rho a_i L_o^2}{210} & 0 & 0 & 0 & \frac{9\rho a_i L_o}{70} & 0 & -\frac{13\rho a_i L_o^2}{420} & 0 \\ 0 & 0 & 0 & \frac{\rho J_i L_o}{3} & 0 & 0 & 0 & 0 & 0 & \frac{\rho J_i L_o}{6} & 0 & 0 \\ 0 & 0 & -\frac{11\rho a_i L_o^2}{210} & 0 & \frac{\rho a_i L_o^3}{105} & 0 & 0 & 0 & -\frac{13\rho a_i L_o^2}{420} & 0 & \frac{3\rho a_i L_o^3}{420} & 0 \\ 0 & \frac{11\rho a_i L_o^2}{210} & 0 & 0 & 0 & \frac{\rho a_i L_o^3}{105} & 0 & \frac{13\rho a_i L_o^2}{420} & 0 & 0 & 0 & -\frac{3\rho a_i L_o^3}{420} \\ \frac{\rho a_i L_o}{6} & 0 & 0 & 0 & 0 & 0 & \frac{\rho a_i L_o}{3} & 0 & 0 & 0 & 0 & 0 \\ 0 & \frac{9\rho a_i L_o}{70} & 0 & 0 & 0 & \frac{13\rho a_i L_o^2}{420} & 0 & \frac{13\rho a_i L_o}{35} & 0 & 0 & 0 & -\frac{11\rho a_i L_o^2}{210} \\ 0 & 0 & \frac{9\rho a_i L_o}{70} & 0 & -\frac{13\rho a_i L_o^2}{420} & 0 & 0 & 0 & \frac{13\rho a_i L_o}{35} & 0 & \frac{11\rho a_i L_o^2}{210} & 0 \\ 0 & 0 & 0 & \frac{\rho J_i L_o}{6} & 0 & 0 & 0 & 0 & 0 & \frac{\rho J_i L_o}{3} & 0 & 0 \\ 0 & 0 & \frac{13\rho a_i L_o^2}{420} & 0 & -\frac{3\rho a_i L_o^3}{420} & 0 & 0 & 0 & \frac{11\rho a_i L_o^2}{210} & 0 & \frac{\rho a_i L_o^3}{105} & 0 \\ 0 & -\frac{13\rho a_i L_o^2}{420} & 0 & 0 & 0 & -\frac{3\rho a_i L_o^3}{420} & 0 & -\frac{11\rho a_i L_o^2}{210} & 0 & 0 & 0 & \frac{\rho a_i L_o^3}{105} \end{bmatrix}. \quad (A.4)$$

A.5. The Mass Matrix for the Rotational Inertia

$$\mathbf{m}_2 = \begin{bmatrix} 0 & 0 & 0 & 0 & 0 & 0 & 0 & 0 & 0 & 0 & 0 & 0 \\ 0 & \frac{42\rho I_{zi}}{35L_o} & 0 & 0 & 0 & \frac{\rho I_{zi}}{10} & 0 & -\frac{42\rho I_{zi}}{35L_o} & 0 & 0 & 0 & \frac{\rho I_{zi}}{10} \\ 0 & 0 & \frac{42\rho I_{y_i}}{35L_o} & 0 & -\frac{\rho I_{y_i}}{10} & 0 & 0 & 0 & -\frac{42\rho I_{y_i}}{35L_o} & 0 & -\frac{\rho I_{y_i}}{10} & 0 \\ 0 & 0 & 0 & 0 & 0 & 0 & 0 & 0 & 0 & 0 & 0 & 0 \\ 0 & 0 & -\frac{\rho I_{y_i}}{10} & 0 & \frac{2\rho I_{y_i}L_o}{15} & 0 & 0 & 0 & \frac{\rho I_{y_i}}{10} & 0 & -\frac{\rho I_{y_i}L_o}{30} & 0 \\ 0 & \frac{\rho I_{zi}}{10} & 0 & 0 & 0 & \frac{2\rho I_{zi}L_o}{15} & 0 & -\frac{\rho I_{zi}}{10} & 0 & 0 & 0 & -\frac{\rho I_{zi}L_o}{30} \\ 0 & 0 & 0 & 0 & 0 & 0 & 0 & 0 & 0 & 0 & 0 & 0 \\ 0 & -\frac{42\rho I_{zi}}{35L_o} & 0 & 0 & 0 & -\frac{\rho I_{zi}}{10} & 0 & \frac{42\rho I_{zi}}{35L_o} & 0 & 0 & 0 & -\frac{\rho I_{zi}}{10} \\ 0 & 0 & -\frac{42\rho I_{y_i}}{35L_o} & 0 & \frac{\rho I_{y_i}}{10} & 0 & 0 & 0 & \frac{42\rho I_{y_i}}{35L_o} & 0 & \frac{\rho I_{y_i}}{10} & 0 \\ 0 & 0 & 0 & 0 & 0 & 0 & 0 & 0 & 0 & 0 & 0 & 0 \\ 0 & 0 & -\frac{\rho I_{y_i}}{10} & 0 & -\frac{\rho I_{y_i}L_o}{30} & 0 & 0 & 0 & \frac{\rho I_{y_i}}{10} & 0 & \frac{2\rho I_{y_i}L_o}{15} & 0 \\ 0 & \frac{\rho I_{zi}}{10} & 0 & 0 & 0 & -\frac{\rho I_{zi}L_o}{30} & 0 & -\frac{\rho I_{zi}}{10} & 0 & 0 & 0 & \frac{2\rho I_{zi}L_o}{15} \end{bmatrix}. \tag{A.5}$$

Data Availability

The data used to support the findings of this study are available from the corresponding author upon request.

Conflicts of Interest

The authors declare that they have no conflicts of interest.

References

[1] A. K. Naik, M. Nazeer, D. Prasad, T. Laha, and S. Roy, "Development of functionally graded ZrB2–B4C composites for lightweight ultrahigh-temperature aerospace applications," *Ceramics International*, vol. 48, no. 22, pp. 33332–33339, 2022.

[2] Z. Zhang, L. Zhang, B. Song, Y. Yao, and Y. Shi, "Bamboo-inspired, simulation-guided design and 3D printing of light-

weight and high-strength mechanical metamaterials," *Applied Materials Today*, vol. 26, Article ID 101268, 2022.

[3] M. Shadlou, W. Sun, and T. Lou, "A novel FRP composite with high-strength, high extensibility in tension: 1-D constitutive relation," *Composite Structures*, vol. 261, Article ID 113332, 2021.

[4] J. Leng, Q. Wang, and Y. Li, "A geometrically nonlinear analysis method for offshore renewable energy systems—examples of offshore wind and wave devices," *Ocean Engineering*, vol. 250, Article ID 110930, 2022.

[5] P. A. Trapper, "A numerical model for geometrically nonlinear analysis of a pipe-lay on a rough seafloor," *Ocean Engineering*, vol. 252, Article ID 111146, 2022.

[6] Y. Liu, *"The development of the co-rotational finite element for the prediction of the longitudinal load factor for a transmission line system,"* PhD Thesis, The University of Manitoba, Winnipeg, Manitoba, 2014.

[7] Q. Xiaohang, G. Zhiteng, W. Tongguang, W. Long, and K. Shitang, "Nonlinear aeroelastic response analysis of 100-meter-scale flexible wind turbine blades," *Acta Aerodynamica Sinica*, vol. 40, pp. 220–230, 2022.

[8] T. W. Liu and J. B. Bai, "Folding behaviour of a deployable composite cabin for space habitats-part 1: experimental and numerical investigation," *Composite Structures*, vol. 302, Article ID 116244, 2022.

[9] M. A. Crisfield, *Non-linear Finite Element Analysis of Solids and Structures*, Jon Wiley & Sons, West Sussex, UK, 1st edition, 1991.

[10] M. J. Turner, R. W. Clough, H. C. Martin, and L. J. Topp, "Large deflections of structures subjected to heating and external loads," *Journal of the Aerospace Sciences*, vol. 27, pp. 99–106, 1960.

[11] J. H. Argyris, *Recent Advances in Matrix Methods of Structural Analysis*, vol. 4, Pergamon Press, New York, NY, USA, 1964.

[12] J. T. Oden, *Finite Elements of Nonlinear Continua*, McGraw-Hill, New York, NY, USA, 1972.

[13] K. J. Bathe, *Finite Element Procedures*, Prentice Hall, New Jersey, NJ, USA, 1st edition, 1996.

[14] M. V. B. Santana, C. Sansour, M. Hjiaj, and H. Somja, "An equilibrium-based formulation with nonlinear configuration dependent interpolation for geometrically exact 3D beams," *International Journal for Numerical Methods in Engineering*, vol. 123, no. 2, pp. 444–464, 2021.

[15] D. Vo, P. Nanakorn, and T. Q. Bui, "A total Lagrangian Timoshenko beam formulation for geometrically nonlinear isogeometric analysis of spatial beam structures," *Acta Mechanica*, vol. 231, no. 9, pp. 3673–3701, 2020.

[16] J. C. Simo and L. Vu-Quoc, "A three-dimensional finite-strain rod model. Part II: computational aspects," *Computer Methods in Applied Mechanics and Engineering*, vol. 58, no. 1, pp. 79–116, 1986.

[17] S. N. Remseth, "Nonlinear static and dynamic analysis of framed structures," *Computers and Structures*, vol. 10, no. 6, pp. 879–897, 1979.

[18] Y. B. Yang, S. Kuo, and Y. S. Wu, "Incrementally small-deformation theory for nonlinear analysis of structural frames," *Engineering Structures*, vol. 24, no. 6, pp. 783–798, 2002.

[19] Y. B. Yang, S. P. Lin, and C. S. Chen, "Rigid body concept for geometric nonlinear analysis of 3D frames, plates and shells based on the updated Lagrangian formulation," *Computer Methods in Applied Mechanics and Engineering*, vol. 196, no. 7, pp. 1178–1192, 2007.

[20] T. Belytschko and B. Hsieh, "Non-linear transient finite element analysis with convected co-ordinates," *International Journal for Numerical Methods in Engineering*, vol. 7, no. 3, pp. 255–271, 1973.

[21] H. A. Elkaranshawy and M. A. Dokainish, "Corotational finite element analysis of planar flexible multibody systems," *Computers and Structures*, vol. 54, no. 5, pp. 881–890, 1995.

[22] H. A. Elkaranshawy, A. A. H. Elerian, and W. I. Hussien, "A corotational formulation based on Hamilton's principle for geometrically nonlinear thin and thick planar beams and frames," *Mathematical Problems in Engineering*, vol. 2018, Article ID 2670462, 22 pages, 2018.

[23] J. Gu, *"Large displacement elastic analysis of space frames allowing for flexural-torsional buckling of beams,"* PhD Thesis, Hong Kong Polytechnic University, Hong Kong, 2004.

[24] C. Oran, "Tangent stiffness in space frames," *Journal of the Structural Division*, vol. 99, no. 6, pp. 987–1001, 1973.

[25] M. A. Crisfield, "A consistent co-rotational formulation for non-linear, three-dimensional, beam-elements," *Computer Methods in Applied Mechanics and Engineering*, vol. 81, no. 2, pp. 131–150, 1990.

[26] T. N. Le, J. M. Battini, and M. Hjiaj, "A consistent 3D corotational beam element for nonlinear dynamic analysis of flexible structures," *Computer Methods in Applied Mechanics and Engineering*, vol. 269, pp. 538–565, 2014.

[27] J. B. Jonker and J. P. Meijaard, "A geometrically non-linear formulation of a three-dimensional beam element for solving large deflection multibody system problems," *International Journal of Non-Linear Mechanics*, vol. 53, pp. 63–74, 2013.

[28] K. M. Hsiao, J. Y. Lin, and W. Y. Lin, "A consistent co-rotational finite element formulation for geometrically non-linear dynamic analysis of 3-D beams," *Computer Methods in Applied Mechanics and Engineering*, vol. 169, no. 1-2, pp. 1–18, 1999.

[29] K. J. Bathe and S. Bolourchi, "Large displacement analysis of three-dimensional beam structures," *International Journal for Numerical Methods in Engineering*, vol. 14, no. 7, pp. 961–986, 1979.

[30] A. C. Benjamin, "Análise Não-Linear Geométrica De Pórticos Tridimensionais Pelo Método Dos Elementos Finitos," M.Sc. thesis, Rio de Janeiro, Brasil, 1982.

[31] C. C. Nunes, H. L. Soriano, and F. filho, "Geometric non-linear analysis of space frame with rotation greater than 90°, with Euler angles and quasi-fixed local axes system," *International Journal of Non-Linear Mechanics*, vol. 38, no. 8, pp. 1195–1204, 2003.

[32] S. Caddemi and A. Morassi, "Multi-cracked Euler–Bernoulli beams: mathematical modeling and exact solutions," *International Journal of Solids and Structures*, vol. 50, no. 6, pp. 944–956, 2013.

[33] S. Caddemi, I. Calio, and M. Marletta, "The non-linear dynamic response of the Euler–Bernoulli beam with an arbitrary number of switching cracks," *International Journal of Non-linear Mechanics*, vol. 45, no. 7, pp. 714–726, 2010.

[34] A. Beheshti, "Large deformation analysis of strain-gradient elastic beams," *Computers and Structures*, vol. 177, pp. 162–175, 2016.

[35] S. L. Chan, "Large deflection kinematic formulations for three-dimensional framed structures," *Computer Methods in Applied Mechanics and Engineering*, vol. 95, no. 1, pp. 17–36, 1992.

[36] H. Goldstein, C. Poole, and J. Safko, *Classical Mechanics*, Addison-Wesley, Boston, MA, USA, 1980.

[37] A. A. Shabana, *Dynamics of Multibody Systems*, Cambridge University Press, Cambridge, UK, 2020.
[38] N. M. Newmark, "A method of computation for structural dynamics," *Journal of the Engineering Mechanics Division*, vol. 85, no. 3, pp. 67–94, 1959.
[39] D. P. Mondkar and G. H. Powell, "Finite element analysis of non-linear static and dynamic response," *International Journal for Numerical Methods in Engineering*, vol. 11, no. 3, pp. 499–520, 1977.
[40] S. L. Chan, "Large deflection dynamic analysis of space frames," *Computers and Structures*, vol. 58, no. 2, pp. 381–387, 1996.
[41] K. Behdinan, M. C. Stylianou, and B. Tabarrok, "Co-rotational dynamic analysis of flexible beams," *Computer Methods in Applied Mechanics and Engineering*, vol. 154, no. 3-4, pp. 151–161, 1998.
[42] J. C. Simo and L. Vu-Quoc, "On the dynamics in space of rods undergoing large motions—a geometrically exact approach," *Computer Methods in Applied Mechanics and Engineering*, vol. 66, no. 2, pp. 125–161, 1988.